

Article

Single- and Multi-Objective Optimization Frameworks of Shape Design of Tubular Linear Synchronous Motor

Araby Mahdy¹, Abdullah Shaheen² , Ragab El-Sehiemy^{3,*} , Ahmed Ginidi²  and Saad F. Al-Gahtani⁴ ¹ Department of Mechanical Engineering, Faculty of Engineering, Suez University, Suez 43533, Egypt² Department of Electrical Engineering, Faculty of Engineering, Suez University, Suez 43533, Egypt³ Department of Electrical Engineering, Faculty of Engineering, Kafrelsheikh University, Kafrelsheikh 33516, Egypt⁴ Department of Electrical Power Engineering, Faculty of Engineering, King Khalid University, Abha 61421, Saudi Arabia

* Correspondence: elsehiemy@eng.kfs.edu.eg

Abstract: The shape design of the Tubular Linear Synchronous Motor (TLSM) is a critical engineering optimization problem which was handled as single- and multi-objective optimization frameworks. However, the different practical constraints for the TLSM design must be efficiently guaranteed. This paper proposes a developed multi-objective shape design of the TLSM to maximize the operating force and minimize the flux saturation. In this regard, a Multi-objective Grey Wolf Optimizer (MGWO) is developed, including an outside archive with a predetermined size that is integrated for storing and retrieving Pareto optimal solutions. Using this knowledge, the grey wolf social structure would then be established, and, in the multi-objective searching environments, grey wolf hunting behavior would then be replicated. The superiority and effectiveness of the developed MGWO is assessed in comparison to the Multi-objective Flower Pollination Algorithm (MFWA), Multi-objective Lichtenberg Algorithm (MOLA), and Multi-objective Grasshopper Optimization Algorithm (MGOA). The outcomes illustrate that the developed MGWO provides an average improvement of 73.46%, 19.07%, and 15.15% compared to MFWA, MOLA, and MGOA, respectively. The validation of the developed MGWO is extended for a multi-objective form of welded beam design (WBD) by simultaneously minimizing the deflection and the manufacturing costs. Similar findings are obtained with different reference points, the developed MGWO provides an average improvement of 2.8%, 0.7%, and 3.04% compared to MFWA, MOLA, and MGOA, respectively.

Keywords: grey wolf algorithm; pareto archive; multi-objective shape design of tubular linear synchronous motor; maximizing the operating force; minimizing the flux saturation



Citation: Mahdy, A.; Shaheen, A.; El-Sehiemy, R.; Ginidi, A.; Al-Gahtani, S.F. Single- and Multi-Objective Optimization Frameworks of Shape Design of Tubular Linear Synchronous Motor. *Energies* **2023**, *16*, 2409. <https://doi.org/10.3390/en16052409>

Academic Editor: Abu-Siada Ahmed

Received: 4 February 2023
Revised: 23 February 2023
Accepted: 28 February 2023
Published: 2 March 2023



Copyright: © 2023 by the authors. Licensee MDPI, Basel, Switzerland. This article is an open access article distributed under the terms and conditions of the Creative Commons Attribution (CC BY) license (<https://creativecommons.org/licenses/by/4.0/>).

1. Introduction

Nature presents several multi-objective design problems in the real world. Even for scientists and engineers with a wide range of specialties, multi-objective optimization problems have become quite important. Nonetheless, despite significant progress, the robustness and effectiveness of existing techniques for addressing multi-objective optimization issues remained largely insufficient [1]. As a result, there is constant space for improvement. This is required for multi-objective optimization problems to continue to be an interesting study topic.

Swarm intelligence, evolutionary algorithms, physics-based techniques, and human-based algorithms make up the four fundamental categories of meta-heuristic methods. At first, swarm intelligence approaches, such as particle swarm optimization (PSO) [1], jellyfish search technique [2,3], Aquila optimization algorithm [4,5], hunter prey-based optimization [6,7], gorilla troops algorithm [8], and honey badger algorithm [9,10], have been inspired by swarming and animal group behaviors. Second, evolutionary computer algorithms have been developed based on the representation of biological evolutionary aspects,

such as crossovers, mutations, and selections [11–13]. Additionally, physics-based techniques are motivated by physical laws, such as Archimedes optimization algorithm [14,15], electromagnetism-like algorithm [16], big bang-big crunch algorithm [17], and gravitational search algorithm [18], Henry gas solubility method [19], and motivate physics-based strategies. Finally, human behavior and evolution provide people the ability to become quite familiar with their environments, leading to the development of human-inspired optimizers, such as heap-based optimizers [20], teaching learning-based optimization [21], imperialist competitive algorithms [22], and social network search techniques [23].

In recent years, multi-objective optimization techniques have evolved dramatically. They attempt to provide a range of benefits, including the capacity to identify multiple solving options inside a single test, non-reliance on derivatives, quick convergence, precise Pareto-optimal set, and exhibiting the flexibility in managing both continuous and combinatorial parameters simultaneously with ease [24]. They also aim to make people less vulnerable to the form or continuity of the Pareto front [25]. To solve the multi-objective optimization challenges, several evolutionary strategies have been investigated [26–30]. Rizk-Allah et al. [31] presented a multi-objective fruit fly technique to solve the TLSM optimizing design. The fruit fly algorithm is initially started using a swarm of randomly selected fruit flies. During the early stages, the nearest non-dominated fruit fly assumes the role of the dominated individual. The fruit flies eventually engage in an evolutionary process by arbitrarily moving around the non-dominant alternative for each target. After that, either from the prior non-dominated position or the reference point, the fruit flies are upgraded to the closest place. The reference point is utilized to emphasize the convergence of the non-dominated alternatives, and the weighted sum approach has been included to modify the prior optimal positions of fruit flies. Despite its significant application in acquiring diversified Pareto solutions, its ability to meet design restrictions was called into doubt. The JAYA optimization algorithm has been utilized by Rao et al. in [32] to optimize several design constraints where its strategy combines the global optimal solution attraction of swarm intelligent techniques with the strongest survival concept of evolutionary algorithms. To solve three mechanical design issues and come up with the optimum gear train design, WBD, and tension/compression spring, a butterfly method was created and enhanced by Arora et al. in [33]. This algorithm includes an exploitation phase of advancement, which delivers solutions that give extra opportunities to enhance themselves. On the other side, both studies [32,33] were dealing with the WBD in a single-objective minimization model.

Yang et al. [34] introduced a Multi-objective Flower Pollination Algorithm (MFPA), which was inspired by the pollination process of flowering species. Pereira et al. [35] presented a Multi-objective Lichtenberg Algorithm (MOLA), which draws inspiration from Lichtenberg patterns and the spread of radial intra-cloud lightning. Since it dispenses the locations to be assessed in the fitness function under a Lichtenberg graph, which is snapped in dimensions and distinct rotations at every iteration, the technique calculates in its optimization workout a combination system relying on both the population and the trajectory, exhibiting a remarkable ability for exploitation and exploration. Mirjalili et al. [36] introduced a Multi-objective Grasshopper Optimization Algorithm (MGOA) inspired by grasshopper swarm navigation in nature. Inside the swarm, the interaction between grasshoppers comprises forces of repulsion and attraction, and safe zones. Additionally, the Pareto optimum front for multi-objective problems is therefore estimated using an archiving and target-choosing strategy included in the algorithm.

The grey wolf social structure and hunting methods are simulated by GWA. Grey wolves' primary hunting techniques include searching for their target, encircling, and attacking their prey. GWA has several unique features of simplicity, convergence speed, and effectiveness, which makes it an application tool for several engineering problems, such as transport network optimization [37], solid oxide fuel cell representation model [38], forecasting the carbon price [39], localization stability improvement and error minimization

of wireless sensor networks [40], energy consumption estimation of electric buses [41], and coordination of static reactive power devices in distribution networks [42].

The metaheuristic optimization problem is an interesting research topic, which has been widely utilized in mechanical engineering and smart materials. Ding et al. [43] suggested a harmony search algorithm searching for the optimum design of flexure-based mechanism for non-circular diamond turning operation. Additionally, Yang et al. [44] provides an efficient application of PSO in order to optimally identify the Preisach model parameters for piezoelectric actuators. To design a MGWO, an exterior repository with a predefined size, as a non-dominated Pareto set, is added [45]. The exterior repository is a straightforward storage mechanism that could store or recover existing Pareto non-dominated solutions. A controlling approach that manages the repository whenever a solution wishes to access the archiving or when it is completed is its primary module. The exterior repository can only have a certain number of members. The current non-dominated alternatives are contrasted to the repository population throughout the repetition process.

1.1. Proposed Novelty of This Research

In this study, a Multi-Objective Grey Wolf Optimization (MGWO) for the Multi-Objective Shape Design of Tubular Linear Synchronous Motors is developed. For storing and retrieving Pareto optimal solutions, the MGWO includes an outside archive with a predetermined size built in. The social structure of grey wolves would then be established using this data, and multi-objective search settings would be used to model grey wolf hunting behavior. By maximizing the operating force and limiting the flux saturation, TLSMs can manage the multi-objective form design. The developed MGWO is compared to several recent algorithms of MFPA, MOLA, and MGOA. The superiority and effectiveness of the developed MGWO, compared to MFPA, MOLA and MGOA, is demonstrated in terms of their single-objective and multi-objective optimization frameworks for TLSM engineering problem. The results clearly indicate how efficient the proposed MGWO is at locating non-dominated solutions. When compared to MFPA, MOLA, and MGOA, the developed MGWO retains an average improvement of 73.46%, 19.07%, and 15.15%, respectively. The validation of the proposed MGWO is expanded to a multi-objective form of welded beam design (WBD) by minimizing deflection and manufacturing costs at the same time. Similar outcomes have been achieved with different reference points; the proposed MGWO yields an average improvement of 2.8%, 0.7%, and 3.04%, when compared to MFPA, MOLA, and MGOA, respectively.

1.2. Key Contribution of the Paper

The key contribution points in this paper can be classified into two categories:
From engineering point of view:

- A developed MGWO is mathematically employed and developed for the multi-objective shape design of TLSM and WBD issues;
- All engineering design constraints are satisfied based on the developed MGWO in contrast to the multi-objective fruit fly method [31].

From mathematical point of view:

- When comparing GWA to FPA, LA, and GOA for both design problems, single-objective optimization frameworks, GWA offers higher superiority, better convergence, and greater robustness;
- Higher hypervolume indications show that the created MGWO outperforms the MFPA, MOLA, and MGOA when different reference points are taken into account for both design problems;
- Furthermore, the proposed MGWO demonstrates greater efficiency and superiority versus true fronts of NSGA II, MFPA, MOLA, and MGOA for WBD based on different metrics presented in the literature, such as hypervolume, generational distance, inverted generational distance, spread, generalized-spread, and additive epsilon.

2. Multi-Objective Shape Design of Tubular Linear Synchronous Motor

2.1. Tubular Linear Synchronous Motor's Basic Configuration

A TLSM's arrangement is depicted in Figure 1 [46,47]. The conductors create rings in the slots of the hollow cylinder that serves as the armature. A little part made of magnets moves within that armature. The cross-sectional images of the TLSM for big and small sizes are depicted in Figures 2 and 3 [31]. The interplay of the magnetic field and currents results in the magnetic force. Flux density, conductor length, and current flowing through the conductors are multiplied together to produce the magnetic force.

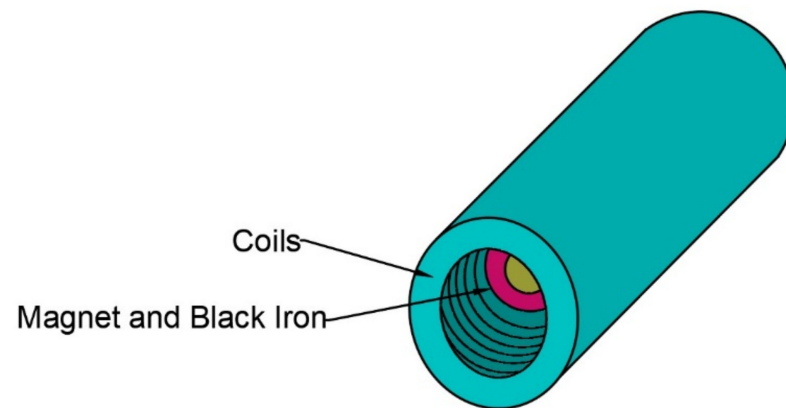


Figure 1. TLSM with stationary coils and a moving magnet [46,47].

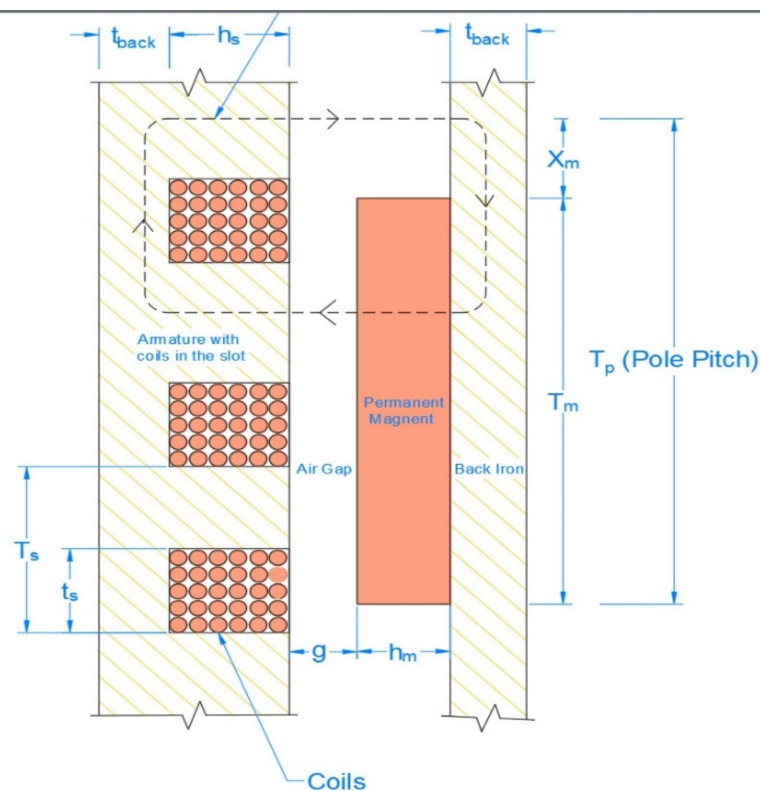


Figure 2. TLSM cross-section [31].

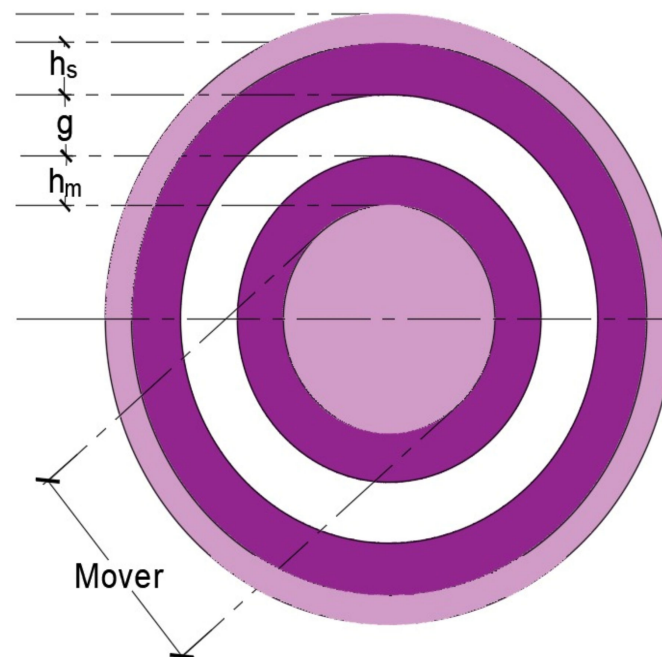


Figure 3. TLSM's cross-section around one pole pitch long [31].

2.2. Design Assessment of TLSM

The current flowing through each slot, its size, and the magnet's height are the pertinent regulatory design variables. The settings of these design variables are constrained by the existing design. The current flowing through each slot is indicated in amperes (A), the density of the flux is indicated in tesla (T), and the lengths are represented in meters (m). Reconsidering the following presumptions for the TLSM design issue:

- Copper is thought to be the main component of conductors;
- Iron Boron magnets with high-density Neodmium would be used as permanent magnets;
- The fill factor k_F is equal to 0.6;
- The air gap width is selected at the shortest permitted value, taking into account production issues (1 mm);
- The magnetic force produced by the TLSM only fluctuates to the amount the flux density (B), length of magnetic pole (l), or current in the conductor (I) and fluctuates with the number of poles (p); it does not explicitly depend on the pole pitch (τ_p);
- Due to manufacturing constraints, the magnet spacing is roughly double the gap width, resulting in a pole pitch that is significantly lower than the 25 mm limit. Therefore, the number of poles is selected to be 40, and the pole pitch is 27 mm because the number of poles must be an even integer, and because the overall length is 1.09 m;
- Both the height of the magnet and the height of the slot are constrained by the motor's radius. The slot thickness can be up to one-third the pole pitch thick;
- A maximum heat dissipation rate of 4000 W is taken into consideration.

2.3. TLSM Design Objectives Optimization

The goal is to design a direct-drive electric actuator to replace the current hydraulic cylinder drive of a submarine's Universal Modular Mast, or periscope component. The present hydraulic cylinder measures about 4 m in length and 16 cm in diameter. However, the potential actuator must have a stroke of roughly 3 m, resulting in an actual permissible length for the actuator of 1.09 m [31]. The present hydraulic actuator raises the mast into the desired position via a pulley/cable system. During different phases of operation, it produces forces spanning from 13,000 N to 30,000 N. Alternatives to hydraulic actuation must work within the current hydraulic cylinder envelope and produce comparable forces.

The design challenge can be phrased as follows and is known as an optimization problem [47]. To optimize the TLSM design as provided in Equations (1) and (2), two objective functions are taken into consideration. The first objective function, which is expressed as “decrease saturation”, and the second objective function, “maximize magnetic force”, are equivalent.

$$\text{Minimize } F_1(x) = 165.13 \times t_s + \frac{1.3 \times h_m}{0.00117 + h_m} \quad (1)$$

$$\text{Maximize } F_2(x) = \frac{653.451 \times h_m \times ins \times (h_m + \frac{h_s}{2} + 0.02825)}{0.00117 + h_m} \quad (2)$$

where, $F_1(x)$ is the flux saturation; t_s indicates the slot thickness; h_m refers to the height of the magnet; $F_2(x)$ is the operating force; h_s is the height of the slot; and ins represents the slot current.

In order to convert the maximization function towards a minimization form, Equation (2) can be multiplied by -1 as follows:

$$\text{Minimize } F_2(x) = - \left[\frac{653.451 \times h_m \times ins \times (h_m + \frac{h_s}{2} + 0.02825)}{0.00117 + h_m} \right] \quad (3)$$

2.4. TLSM Design Constraints Optimization

Owing to resistance losses, the electrical conductors, which carry currents in the armature portion of the TLSM generate heat in order to comply with the heat restriction. The volume space of the conductors and the electrical current passing through them both affect how much heat is produced. As a result, the conductors current and TLSM power are constrained by the thermal dissipation limitation in the following ways:

$$G_1(x) = - \frac{1.92 \times ins^2 \times (h_m + \frac{h_s}{2} + 0.02825)}{t_s \times h_s} \quad (4)$$

where, $G_1(x)$ is the first inequality constraint related to the thermal dissipation limitation.

Second, both the entire radius and the length are restricted for the TLSM in the analysis. The overall radius cap places restrictions on the sizes of various motor parts.

$$G_2(x) = (h_s + h_m) - (0.0266 + 3t_s) \leq 0 \quad (5)$$

where, $G_2(x)$ is the second inequality constraint related to the overall radius cap places restrictions.

Third, the saturation constraint's highest level serves as a restriction as follows:

$$G_3(x) = \frac{1.3h_m}{(0.00117 + h_m)} + (165.13t_s) - 1.5 \leq 0 \quad (6)$$

where, $G_3(x)$ is the third inequality constraint related to the saturation limitation.

Fourth, at specific points during the motor's operation, the armature current field balances the magnetic field. Therefore, the demagnetizing constraint is another restriction on the armature current, as:

$$G_4(x) = \left[\frac{6.28 \times 10^{-7}}{(0.00105 + h_m) \times h_m} \times (0.00105 + h_m) \times ins \right] - 1.17 \leq 0 \quad (7)$$

where, $G_4(x)$ is the first inequality constraint related to the demagnetizing limitation.

Finally, the minimal force should be limited as follows:

$$G_5(x) = 15 \times 10^3 - \left[\frac{653.451 \times (h_m + \frac{h_s}{2} + 0.02825) \times ins}{(0.00117 + h_m)} \right] \leq 0 \quad (8)$$

where, $G_5(x)$ is the first inequality constraint related to the minimal force limitation.

3. Developed MGWO for Solving Multi-Objective Shape Design of TLSSM

3.1. Grey Wolf Algorithm

The grey wolf social structure and hunting methods are simulated by the GWA. Grey wolves' primary hunting techniques include of searching for their target, surrounding it, then striking it. Alpha (α) is regarded as the strongest dominant participant of the GWA family. The remaining junior participants, known as beta (β) and delta (Δ), assist in regulating the vast bulk of wolves, known as omega (ω). Beta, delta, and alpha possess a greater understanding of the likely position of the target prey. The other wolves in the pack should adjust their placements in view of the top three alternatives since they outperformed all the wolves in the pack, where their total number is indicated by (N_w). These actions can be described as follows [48–50]:

$$\vec{D}_\alpha = \left| -\vec{Y} + \vec{C}_\alpha \vec{Y}_\alpha \right| \quad (9)$$

$$\vec{D}_\beta = \left| -\vec{Y} + \vec{C}_\beta \vec{Y}_\beta \right| \quad (10)$$

$$\vec{D}_\delta = \left| -\vec{Y} + \vec{C}_\delta \vec{Y}_\delta \right| \quad (11)$$

$$\vec{Y}_1 = \vec{Y}_\alpha - \vec{D}_\alpha \vec{A}_1 \quad (12)$$

$$\vec{Y}_2 = \vec{Y}_\beta - \vec{D}_\beta \vec{A}_2 \quad (13)$$

$$\vec{Y}_3 = \vec{Y}_\delta - \vec{D}_\delta \vec{A}_3 \quad (14)$$

$$\vec{Y}_{new} = \frac{\vec{Y}_1 + \vec{Y}_2 + \vec{Y}_3}{3} \quad (15)$$

where the locations of the delta, beta, alpha are represented, respectively, by Y_Δ , Y_β , and Y_α , while their accompanied distances are indicated, respectively, by D_Δ , D_β , and D_α , the distance between the alpha, beta, and delta, respectively. The wolf's new location is Y_{new} , whereas Y refers to its current one.

The following formula is used to determine the vectors of coefficients A and C :

$$\vec{A} = 2\vec{a}r - \vec{a} \quad (16)$$

where,

$$\vec{A} = \vec{A}_1 = \vec{A}_2 = \vec{A}_3 \quad (17)$$

$$\vec{C} = 2r \quad (18)$$

where,

$$\vec{C} = \vec{C}_\alpha = \vec{C}_\beta = \vec{C}_\delta \quad (19)$$

where a randomized value, r , is used.

The next formula describes the linear drop of the coefficient a from 2 to 0:

$$\vec{a} = 2 \cdot \left(1 - \frac{It}{Mx_{It}}\right) \quad (20)$$

where, It represents the existing repetition, and Mx_{It} signifies the ultimate repetition number. Figure 4 displays the basic steps of GWA.

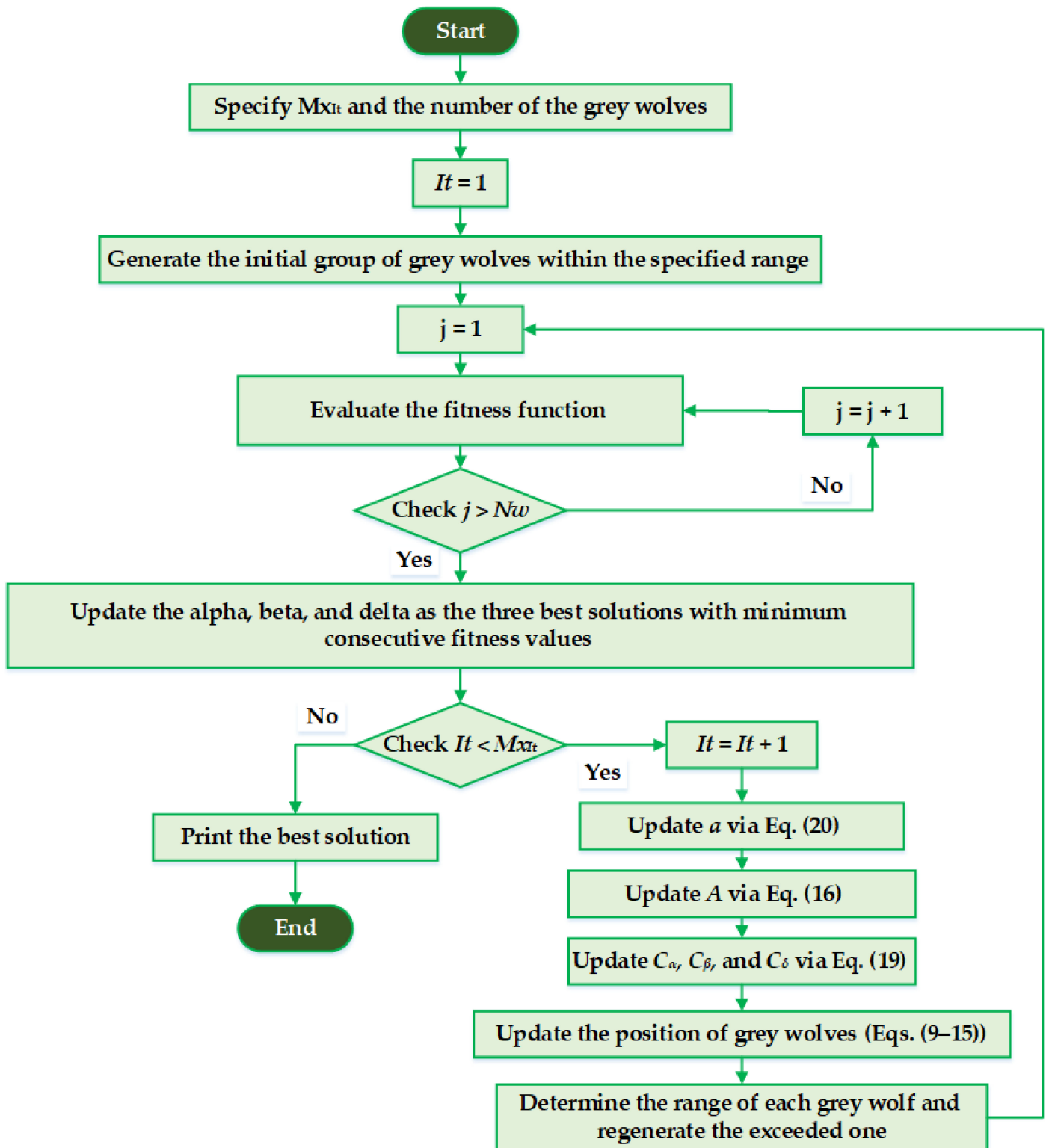


Figure 4. Basic steps of GWA.

As the first population, the GWA begins the optimization journey by producing a group of arbitrary alternatives. The current three top results are stored and referred to as alpha, beta, and delta wolves, respectively, through development. The position

update Formulas (9) through (15) are activated for each omega wolf. In the meantime, over the duration of a repetition, factors a and A are linearly lowered. As a result, based on their changed values, searching wolves prefer to disperse away the target prey and consolidate somewhat on the target prey. Eventually, whenever an end criterion is met, the location and fitness of the alpha option are supplied as the optimal outcomes from the optimization process.

3.2. Developed Multi-Objective Grey Wolf Algorithm for TLSM Design

In order to design a MGWO, an exterior repository with a predefined size, as a non-dominated Pareto set, is added [45]. The exterior repository is a straightforward storage mechanism which could store or recover existing Pareto non-dominated solutions. A controlling approach that manages the repository whenever a solution wishes to access the archiving or when it is completed is its primary module. The exterior repository can only have a certain number of members. The current non-dominated alternatives are contrasted to the repository population throughout the repetition process.

A deleting procedure is carried out after the repository is complete. The most congested sections will be first chosen, and an alternative is arbitrarily removed from any section to make room for the incoming alternative. The insertion of a solution from outside hypercubes is a specific situation [51]. In this instance, all of the portions have been expanded to include the fresh approaches. As a result, other solutions' portions can also be modified.

Additionally, a leader selection approach is the second element, and it helps select alpha, beta, and delta solutions as the process's leaders when searching through the archive. In the GWA, the alpha, beta, and delta are selected as they provide the least fitness value. In the MGWO, the leader picking mechanism selects the search space's least populated areas and presents one of the non-dominated options as an alpha, beta, or delta wolf. For every hypercube, the choice is made using a roulette-wheel approach [52], having the corresponding probability ($Prob_j$):

$$Prob_j = \frac{Fc}{N_j} \quad (21)$$

where, N represents the total quantity of successful Pareto-optimal solutions in the i^{th} sector, and Fc is a fixed value bigger than one.

In order to handle the TLSM design with their bi-objective functions, F_1 and F_2 , as indicated in Equations (1) and (3), have to be addressed concurrently using the suggested framework, according to the limitations stated above in Equations (4)–(8). For every new location of the created grey wolf, both objectives are evaluated. To handle the several limitations, a penalty function (PF) should be estimated and added to both fitness functions as follows:

$$PF = \sum_{j=1}^5 \lambda \times R_j \times G_j(x) \quad (22)$$

where, λ is a penalty factor with value of 10^{15} , and R_j is a binary coefficient that is defined in Equation (23). It has a value of one if the constraint is violated, and so the penalty function will have a high value. The more the number of violated constraints the more the penalty function will be.

$$R_j = \begin{cases} 1 & G_j(x) > 0 \\ 0 & G_j(x) \leq 0 \end{cases} \quad (23)$$

Figure 5 displays the main steps of the Developed MGWO for TLSM Design.

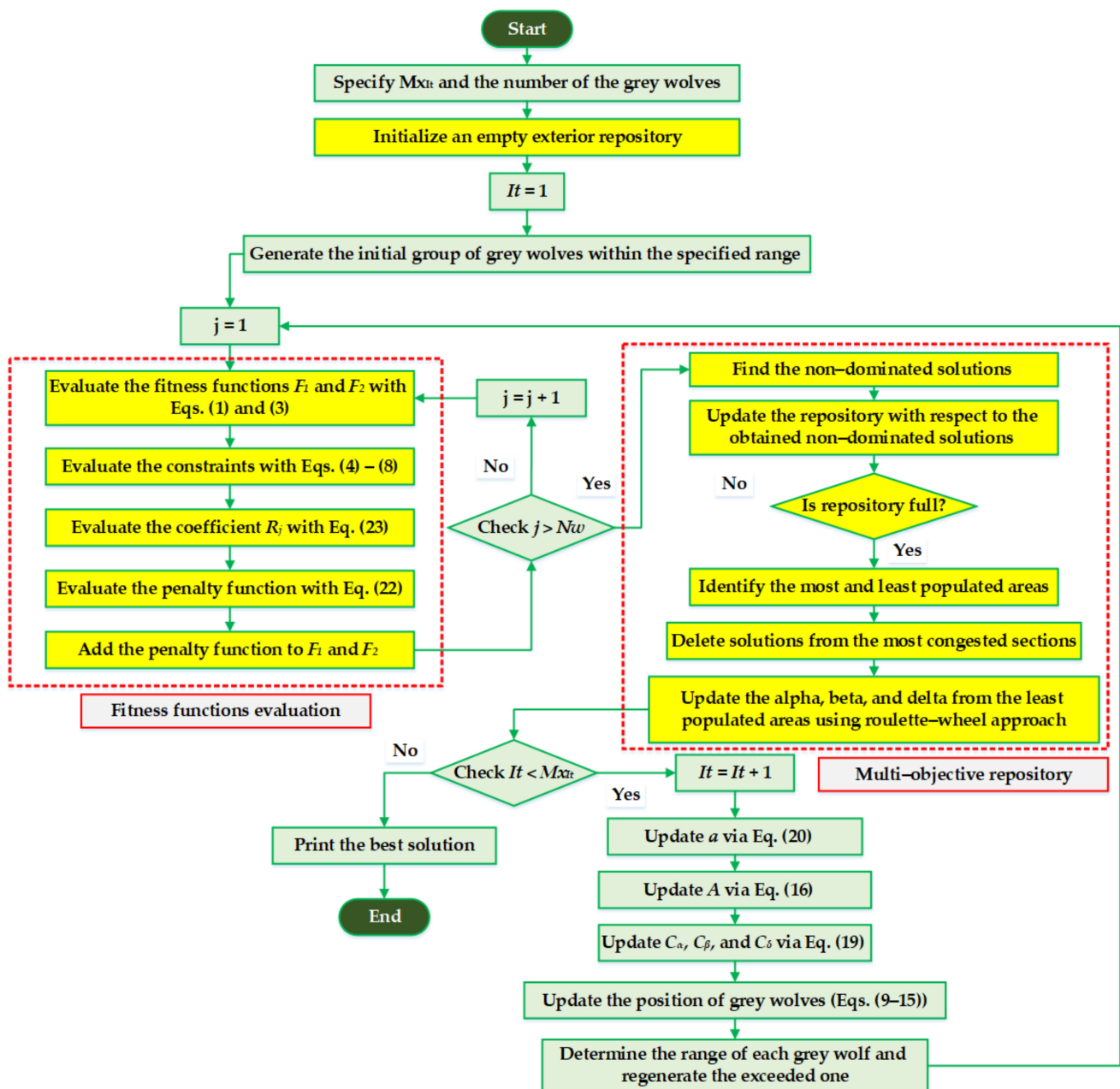


Figure 5. Main steps of the developed MGWO for TLSM design.

4. Simulation Results

In this section, the developed MGWO technique is applied for the multi-objective form design of TLSMs by maximizing the operating force and minimizing the flux saturation. The developed MGWO is compared to several recent algorithms of MFPA [34], MOLA [35], and MGOA [36]. Three different cases are investigated.

In addition, the application of the developed MGWO technique is extended for one of the practical benchmark design problems to optimize the multi-objective form of welded beam design (WBD) by simultaneously minimizing the deflection and the manufacturing costs.

4.1. Applications for TLSM Design

For the TLSM design, three different cases are investigated. In the first and second cases, the assessments of GWA, FPA, LA and GOA are performed in terms of their single-objective optimization frameworks for the TLSM problem. The first case is dedicated

to minimizing the flux saturation described in Equation (1), while the second case is dedicated to maximizing the operating force by minimizing its negative model described in Equation (3). GWA, FPA, LA, and GOA are performed 50 separate times with 100 search agents and 500 repetitions. These circumstances guarantee fair comparisons between them with 50,000 function evaluations. In the third case, the developed MGWO, MFPA, MOLA, and MGOA are performed for the multi-objective optimization framework of the TLSM design by simultaneously minimizing the fitness functions of Equations (1) and (3). The permitted ranges for the control variables are as follows: slot current (i_{ns}) $[0, \infty]$ A, the height of the slot (h_s) $[0, 0.08]$ m, the height of the magnet (h_m) $[0, 0.08]$ m, and slot thickness (t_s) $[0, 0.009]$ m.

4.1.1. First Case: Minimizing the Flux Saturation

Only minimizing the flux saturation described in Equation (1) is treated as a single-objective target in this case. GWA, FPA, LA, and GOA are applied 50 times in this case, and their best results in terms of control variables and outcome fitness values are listed in Table 1.

Table 1. Optimal results of the GWA, FPA, LA, and GOA for TLSM design under first case.

Control Variables	FPA	GOA	LA	GWA
i_{ns} (A)	723.3687	782.4874	806.803	763.6964
h_s (m)	0.002314	0.001812	0.001663	0.001944
h_m (m)	0.034709	0.03644	0.037246	0.035914
t_s (m)	0.00349	0.003894	0.004105	0.003754
F_1 (Saturation)	1.4398	1.4329	1.440899	1.431472

As can be seen, the FPA, LA, and GOA attain values of flux saturation of 1.4398, 1.4329, and 1.440899, respectively, while the GWA achieves the lowest value of 1.4312 for the flux saturation. This indicates the high effectiveness of the GWA in locating the region of the spectrum with the least flux saturation, which was discovered with slot current of 723.3687 A, slot height of 2.314 mm, magnet height of 34.709 mm, and slot thickness of 3.49 mm. Additionally, Figure 6 shows the GWA, FPA, LA, and GOA's best convergence curves.

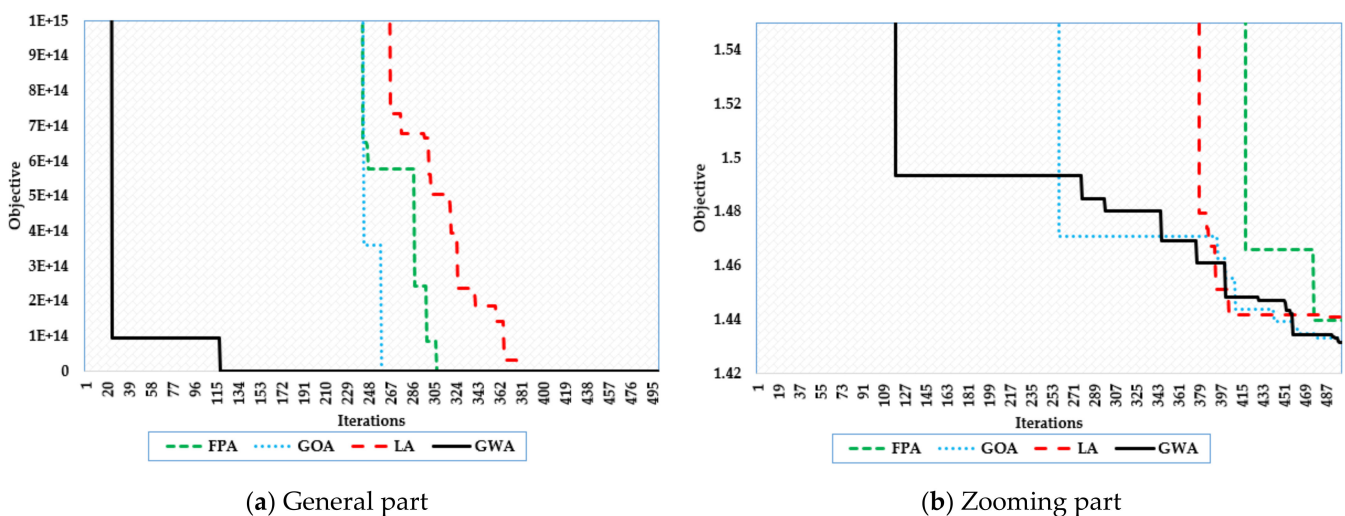


Figure 6. Best Convergence curves of GWA, FPA, LA, and GOA for TLSM design under first case.

From Figure 6, GWA, FPA, LA, and GOA are beginning the search from an extremely high value, which illustrates that all the design constraints are violated. With the progress of the iterations, the GWA shows high speed in maintaining the inequality limitations at

115 iterations. GOA, FPA, and LA are then successfully tackling the inequality constraints after 257, 307, and 380 iterations, respectively.

Figure 7 shows the box and whisker's plot of GWA, FPA, LA, and GOA for TLSM design under the first case to evaluate the robustness of the GWA, FPA, LA, and GOA over the distinct runs. As demonstrated, the GWA performs best across all runs with the lowest values of the evaluated objective. Table 2 presents the robustness indices of the acquired fitness values of GWA, FPA, LA, and GOA to further demonstrate its success. With the smallest indices of 1.431472 as the minimum, 1.43206 as the mean, 1.432432 as the maximum, and 0.000278 as the standard deviation, the GWA in Table 2 exhibits the most resilient behavior.

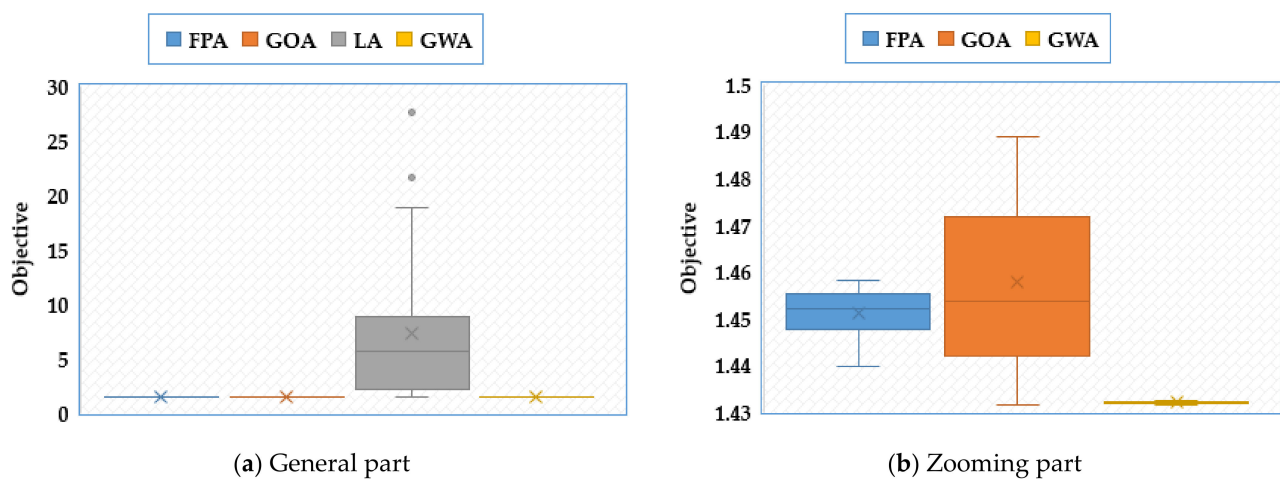


Figure 7. Box and Whiskers plot of GWA, FPA, LA, and GOA for TLSM design under first case.

Table 2. Robustness indices of GWA, FPA, LA, and GOA for TLSM design under first case.

Robustness Indices	FPA	GOA	LA	GWA
Min	1.4398	1.431443	1.440899	1.431472
Mean	1.451078	1.457765	7.347343	1.43206
Max	1.4581	1.488801	27.58696	1.432432
Std	0.004945	0.017357	6.664695	0.000278

In comparison to the reported fruit fly algorithm in [31], Table 3 verifies the constraints justification based on the presented GWA for the TLSM design under the first case. For that, all the constraints are guaranteed using the presented GWA, while two constraints are highly violated due to the reported fruit fly algorithm.

Table 3. Constraints justification based on presented GWA versus Fruit Fly Algorithm [31] for TLSM design under first case.

Design Constraints	Presented GWA	Fruit Fly Algorithm [31]
$G_1(x)$	-0.64478	-3236.93
$G_2(x)$	-4×10^{-6}	-0.0316
$G_3(x)$	-0.06854	0.476092 *
$G_4(x)$	-0.9191	-1.16491
$G_5(x)$	-0.87989	13,416.17 *

* Refers to a violation.

4.1.2. Second Case: Maximizing the Operating Force

Only the maximization of the operating force, as described in Equation (3), is considered a single-objective target. GWA, FPA, LA, and GOA are employed here, and their best control variables and outcome fitness values are displayed in Table 4. Simultaneously, the best convergence curves for the GWA, FPA, LA, and GOA are depicted in Figure 8.

Table 4. Optimal results of the GWA, FPA, LA, and GOA for TLSM design under second case.

Control Variables	FPA	GOA	LA	GWA
i_{ns} (A)	773.0942	787.5933	786.3318	781.7732361
h_s (m)	0.002253	0.002158	0.002157	0.002209554
h_m (m)	0.035994	0.036369	0.036213	0.036195653
t_s (m)	0.003895	0.003978	0.003977	0.003936221
F_2 (Force)	221,216,126.3 *	221,216,217.8 *	221,216,161.23 *	221,216,217.9 *

* Negative sign refers to the handling of the objective in a minimization form.

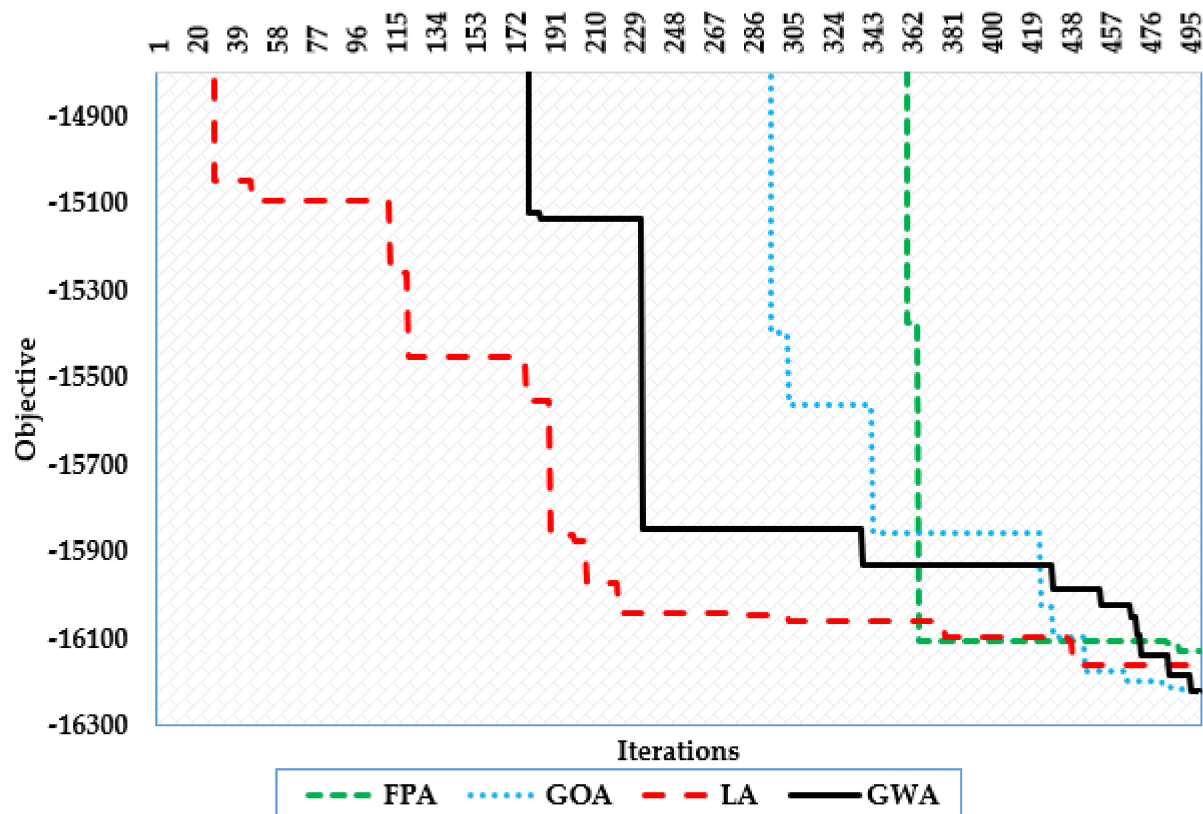


Figure 8. Best Convergence curves of GWA, FPA, LA, and GOA for TLSM design under second case.

As shown, the GWA reaches the lowest value of 16,217.9 N for the flux saturation, while the FPA, LA, and GOA achieve levels of the force of 16,126.3 N, 16,217.8 N, and 16,161.23 N, respectively. With slot current of 781.77 A, slot height of 2.209 mm, magnet height of 36.195 mm, and slot thickness of 3.93 mm, the GWA was highly effective in locating the area of the spectrum with the least flux saturation.

To assess the robustness of the GWA, FPA, LA, and GOA over the various runs, Figure 9 displays the box and whisker's plot of the GWA, FPA, LA, and GOA for the TLSM design under the second case. As shown, the GWA consistently outperforms all other runs with the lowest values of the evaluated objective. To further illustrate its effectiveness, Table 5 provides the robustness indices of the obtained fitness values of GWA, FPA, LA,

and GOA. The minimum, mean, and maximum indices are all the smallest, measuring 16217.888 N, 16206.98 N, and 16199.74 N, respectively. For the standard deviation, the GWA provides the least value of 4.3, while FPA, GOA, and LA deliver counterparts of 92.96, 346.04, and 380.81, respectively. Therefore, the improvement in the standard deviation based on GWA records 96.31%, 98.74%, and 98.85% versus FPA, LA, and GOA, respectively.

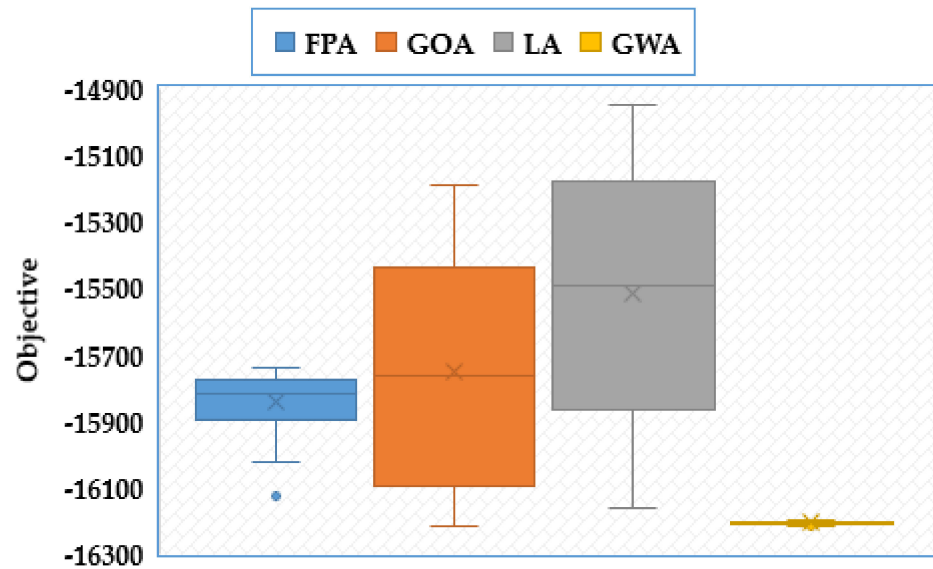


Figure 9. Box and Whiskers plot of GWA, FPA, LA, and GOA for TLSM design under second case.

Table 5. Robustness indices of GWA, FPA, LA, and GOA for TLSM design under second case.

Robustness Indices	FPA	GOA	LA	GWA
Min	-16,126.32831	-16,217.78324	-16,161.23305	-16,217.88823
Mean	-15,845.95082	-15,752.72502	-15,519.26293	-16,206.98609
Max	-15,739.31813	-15,193.0838	-14,949.19667	-16,199.74256
Std	92.96386002	346.0428138	380.808452	4.302506454

Negative sign refers to the handling of the objective in a minimization form.

Table 6 demonstrates the constraints justification based on the presented GWA for the TLSM design under the second case in comparison to the reported fruit fly algorithm in [31]. As a result, the presented GWA guarantees all of the constraints, while the second constraint is slightly violated due to the reported fruit fly algorithm.

Table 6. Constraints justification based on GWA versus Fruit Fly Algorithm [31] for TLSM design under second case.

Design Constraints	Presented GWA	Fruit Fly Algorithm [31]
$G_1(x)$	-0.7165554	-1554.1942
$G_2(x)$	-0.00000345	0.0795 *
$G_3(x)$	-0.0000712	-0.006406
$G_4(x)$	-0.9443427	-1.16793
$G_5(x)$	-1217.888	-2803.1081

* Refers to a violation.

4.1.3. Third Case: Simultaneous Maximizing the Force and Minimizing the Flux Saturation

In the third case, the multi-objective optimization framework of the TLSM design is addressed by simultaneously minimizing the fitness functions of Equations (1) and (3).

The developed MGWO, MFPA, MOLA, and MGOA are performed considering 100 search agents in the exterior repository. The corresponding Pareto fronts are depicted in Figure 10, which illustrates the significant superiority of the developed MGWO in finding better solutions with lower saturations and higher forces in a simultaneous manner compared to the others. To quantify the hypervolume indicator for all the compared methods, a transfer mapping is carried out to the x -axis by adding a positive value of 16,500, and so, Figure 10 will be converted into Figure 11 considering a reference point of (16,000,1.5).

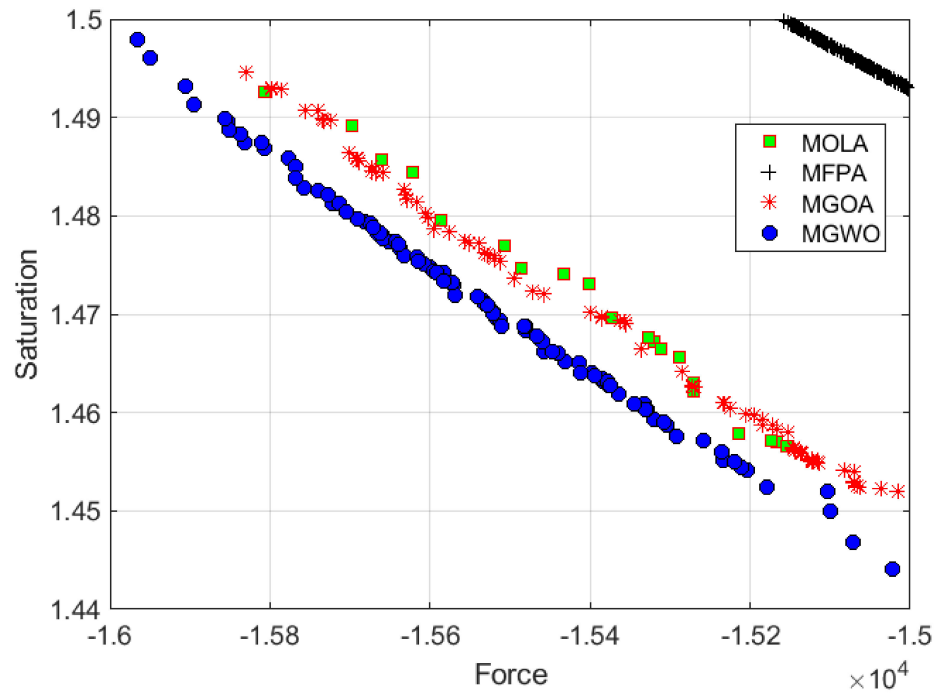


Figure 10. Obtained Pareto fronts of the developed MGWO, MFPA, MOLA, and MGOA for TLISM design under third case.

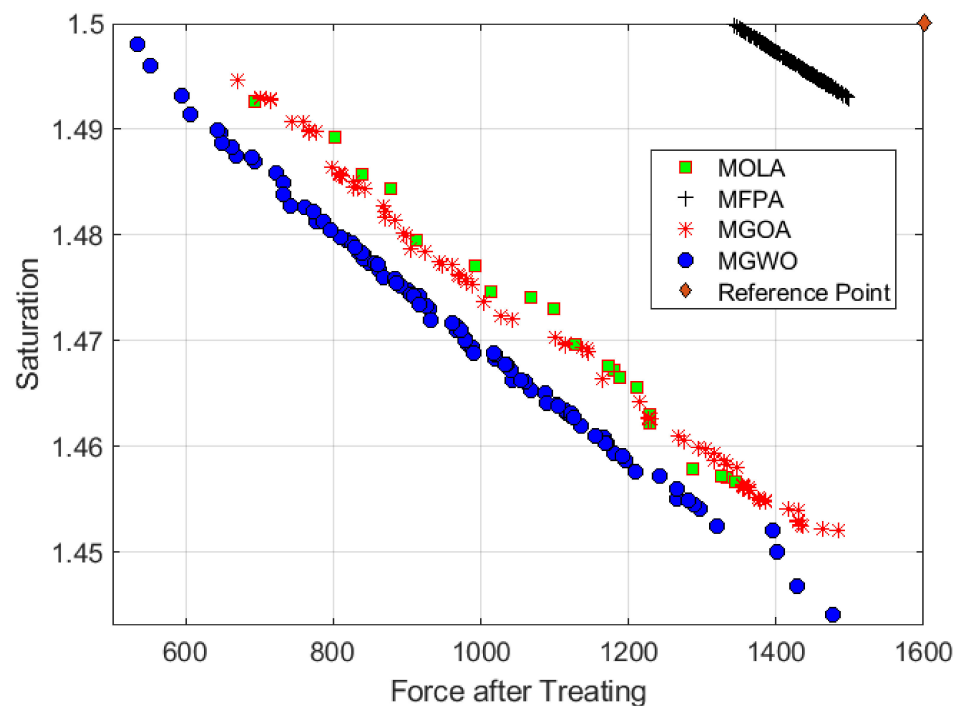


Figure 11. Obtained Pareto fronts of Figure 10 after transfer mapping under third case.

Table 7 displays the hypervolume indicators of the developed MGWO, MFPA, MOLA, and MGOA for the TLSM design in the third case, considering various reference points. As demonstrated, the developed MGWO provides the best performance. In comparison to the MFPA, the developed MGWO provides improvement by 69.49%, 78.41%, and 72.5%, when compared to the reference points (16,000,1.5), (16,500,1.6), and (17,000,1.75), respectively. In comparison to the MOLA, the developed MGWO provides improvement by 25.08%, 17.17%, and 14.98%, respectively, with respect to the reference points. In comparison to the MGOA, the developed MGWO provides improvement by 19.05%, 13.97%, and 12.44%, respectively, with the reference points.

Table 7. Hypervolume indicators of MGWO, MFPA, MOLA, and MGOA for TLSM design under third case.

Reference Points	MFPA	MOLA	MGOA	Developed MGWO
(16000,1.5)	0.000511	0.01093	0.01181	0.01459
Improvement	96.49%	25.08%	19.05%	-
(16500,1.6)	0.01224	0.04696	0.04878	0.0567
Improvement	78.41%	17.17%	13.97%	-
(17000,1.75)	0.03065	0.094795	0.09762	0.1115
Improvement	72.5%	14.98%	12.44%	-

In addition to that, Non-dominated Sorting Genetic Algorithm II (NSGA II) is one of the most applied and successful algorithms in multi-objective optimization in engineering issues [53–55]. It is a genetic algorithm that uses non-dominated sorting and crowding distance to find the Pareto optimal set of solutions for a multi-objective optimization problem. Therefore, a comparative assessment is extended between the proposed MGWO and NSGA II. Figure 12 displays the regarding obtained Pareto set by both the proposed MGWO and the NSGA II.

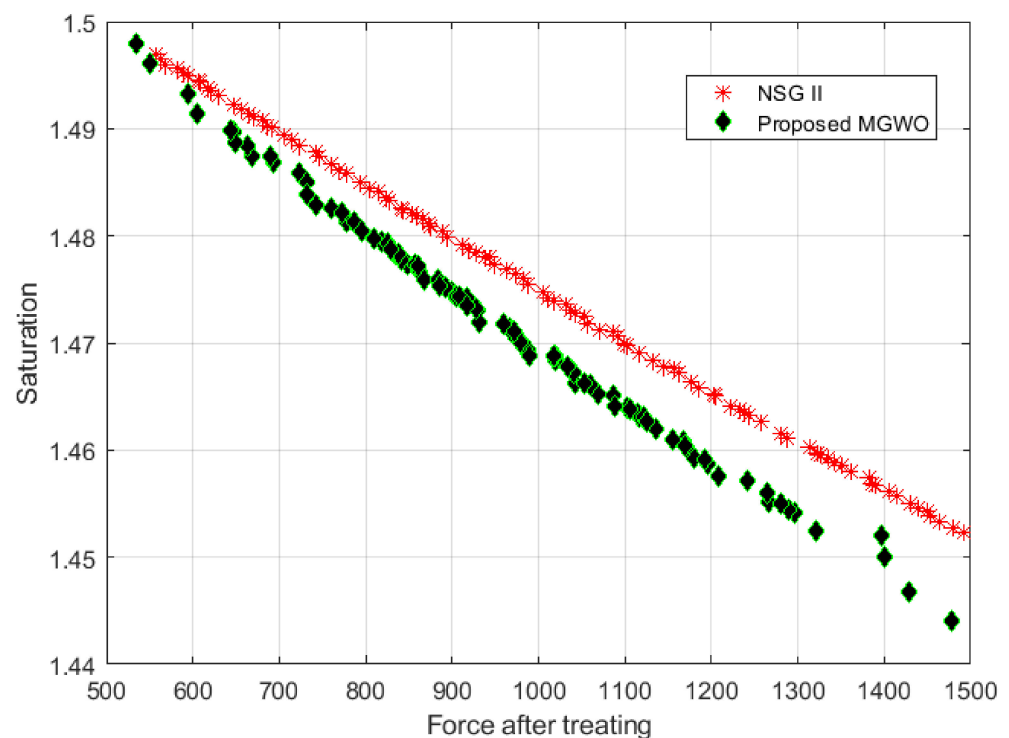


Figure 12. Pareto set via MGWO and NSGA II.

As shown, the proposed MGWO shows higher outperformance compared to the well-known NSGA II since all their obtained solutions show significant dominance compared to their counterparts related to the NSGA II. As can be seen from Figure 12, NSGA II is not always worse than the proposed MGWO, whereas NSGAII always provides better coverage of the PARETO front, as opposed to the gaps observed for the proposed algorithm; however, the proposed MGWO shows higher capability in finding better solutions on the basis of both objectives. The proposed MGWO shows higher capability over NSGA II in finding better solutions that are dominating the counterparts obtained by NSGA II. Table 8 summarizes the corresponding metrics in terms of the minimum, maximum, range, mean, and standard deviation for each objective.

Table 8. MGWO versus NSGA II for TLSM design under third case.

Objective	Saturation			Force after Treating			
	Method	NSGA II	MGWO	Improvement	NSGA II	MGWO	Improvement
minimum		1.4523	1.4441	0.564621635%	558.0469	533.9629	4.315766291%
maximum		1.497973654	1.497005968	0.064599668%	1491.226051	1477.167426	0.942756129%
range		0.04472747902	0.053921415	20.55545312%	933.1791192	943.2045159	1.074327157%
mean		1.475161267	1.471152873	0.271725817%	1000.629818	972.4719583	2.814013654%
standard deviation		0.01340574792	0.01156842432	13.70549119%	279.1829529	212.4380323	23.90723356%

From this table, the proposed MGWA derives higher performance in all metric terms. For the first objective of saturation, the minimum, maximum, range, mean, and standard deviation are improved by 0.56%, 0.06%, 20.56%, 0.27%, and 13.71%, respectively. Additionally, for the second objective, the minimum, maximum, range, mean, and standard deviation are improved by 4.32%, 0.94%, 1.07%, 2.81%, and 23.91%, respectively.

4.2. Applications for Welded Beam Design

The welded beam problem formulation has four design constraints. In this problem, the manufacturing cost of the welding beam (f_1) and its deflection (f_2) should be maintained to a minimum. The four design variables are the weld thickness (x_1), clamping bar length (x_2), bar height (x_3), and bar thickness (x_4). Figure 13 displays a WBD on a substrate [56].

$$\text{Minimize } f_1(x) = 1.1047x_1^2x_2 + 0.04811x_3x_4(14 + x_2) \quad (24)$$

$$\text{Minimize } f_2(x) = \frac{65856000}{30 \times 10^6 \times x_3^3x_4} \quad (25)$$

$$G_1(x) = \tau - 13600 \leq 0 \quad (26)$$

$$G_2(x) = \frac{504000}{x_4x_3^2} - 3000 \leq 0 \quad (27)$$

$$G_3(x) = x_1 - x_4 \leq 0 \quad (28)$$

$$G_4(x) = 6000 - P \leq 0 \quad (29)$$

where,

$$\tau = \sqrt{\left(\frac{6000}{\sqrt{2}x_1x_2}\right)^2 + \frac{2\left(\frac{6000}{\sqrt{2}x_1x_2}\right)\beta x_2}{2R}} + \beta^2 \quad (30)$$

$$\beta = \frac{RM}{J} \quad (31)$$

$$R = \sqrt{\frac{x_2^2}{4} + \left(\frac{x_1 + x_3}{2}\right)^2} \quad (32)$$

$$M = 6000 \left(14 + \frac{x_2}{2} \right) \quad (33)$$

$$J = 2\sqrt{2}x_1x_2 \left[\frac{x_2^2}{12} + \frac{(x_1 + x_3)^2}{4} \right] \quad (34)$$

$$P = 614234.69 \times \sqrt{x_3^2x_4^6/36} \left(1 - \frac{x_3}{28} \sqrt{\frac{30}{48}} \right) \quad (35)$$

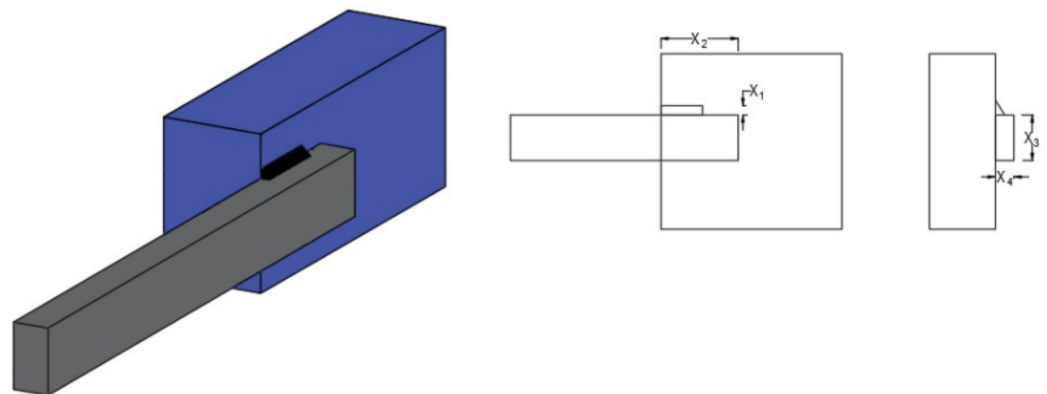


Figure 13. WBD problem [56].

The permitted ranges for the control variables are as follows: weld thickness (x_1) [0.125,5] inches, clamping bar length (x_2) [0.1, 10] inches, bar height (x_3) [0.1, 10] inches, and bar thickness (x_4) [0.125,5] inches. For the WBD problem, three different cases are investigated.

In the first and second cases, the assessment of GWA, FPA, LA, and GOA is performed considering single-objective targets for individually minimizing the manufacturing cost (f_1) and the deflection (f_2), respectively. In the third case, the developed MGWO, MFPA, MOLA, and MGOA are performed for the multi-objective WBD optimization.

4.2.1. First Case: Minimizing the Manufacturing Cost

In this case, GWA, FPA, LA, and GOA are applied to this case for minimizing the manufacturing cost, and their best regarding control variables and outcome fitness values are given in Table 9. The GWA achieves the least expensive value of 1.725. This demonstrates the GWA's superior effectiveness in locating the most cost-effective option, which is attained at a welding thickness of 0.2057 inches, clamping bar length of 3.4715 inches, bar height of 9.035 inches, and bar thickness of 0.20579 inches. Figure 14 also depicts the best convergence curves for the GWA, FPA, LA, and GOA. GWA, FPA, LA, and GOA are starting their searches from quite high values, showing that all of the design limits have been broken. The GWA exhibits impressive speed in maintaining the inequality constraints at only 10 iterations as the iterations progress. The inequality restrictions are then successfully being addressed by GOA, FPA, and LA after 90, 160, and 185 iterations, correspondingly.

Table 9. Optimal results of the GWA, FPA, LA, and GOA for TLSM design under first case.

Control Variables	FPA	GOA	LA	GWA
x_1 (inch)	0.252066308	0.22690479	0.225644069	0.20574862
x_2 (inch)	3.348447907	2.863433027	3.062911117	3.471565595
x_3 (inch)	9.385394959	9.767624642	9.113241032	9.035246022
x_4 (inch)	0.273636448	0.226906446	0.237752691	0.205793087
f_1 (Manufacturing cost)	2.378524018	1.96097676	1.950913074	1.725272522

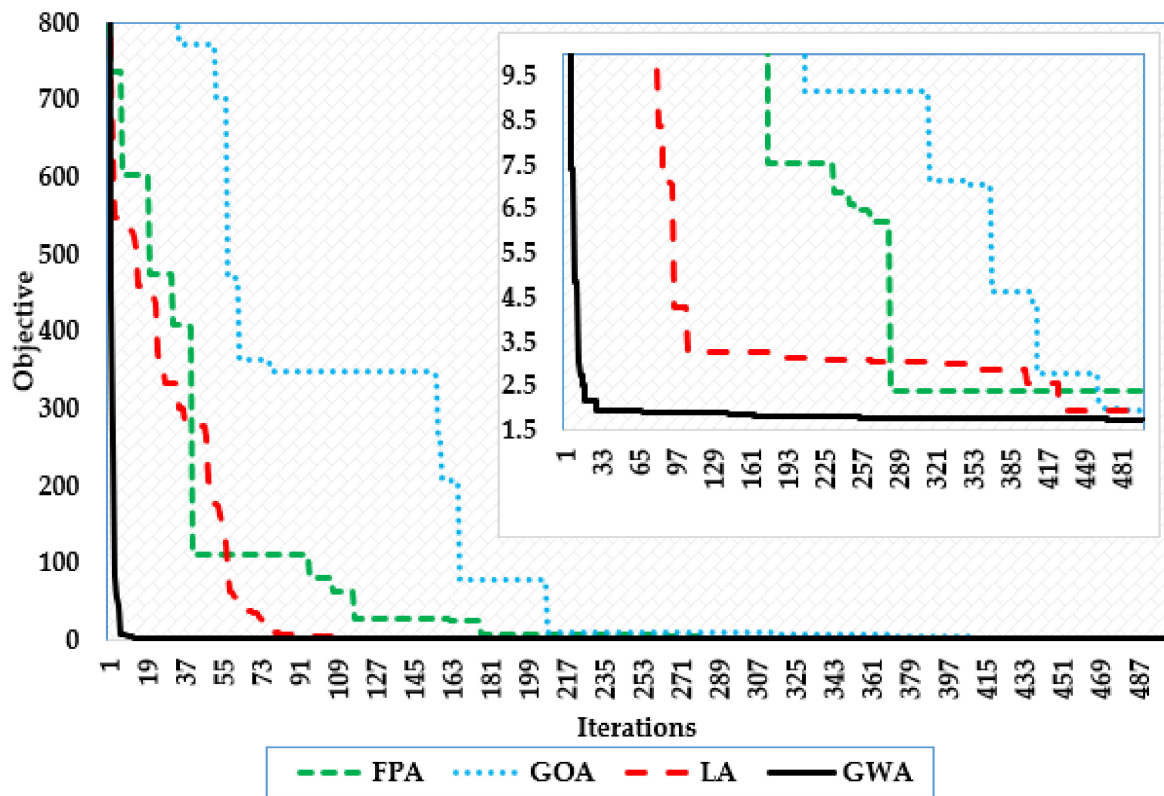


Figure 14. Best Convergence curves of GWA, FPA, LA, and GOA for TLSM design under first case.

Figure 15 shows a statistical assessment of GWA, FPA, LA, and GOA for the WBD problem under the first case. In the first part, the box and whisker’s plot are plotted, which indicates that the GWA performs best across all runs with the lowest values of the evaluated objective. In the second part, the robustness indices are displayed, which declares the high resilience of the GWA since it obtains the smallest indices of 1.7252 as the minimum, 1.7258 as the mean, 1.7263 as the maximum, and 0.000299 as the standard deviation.

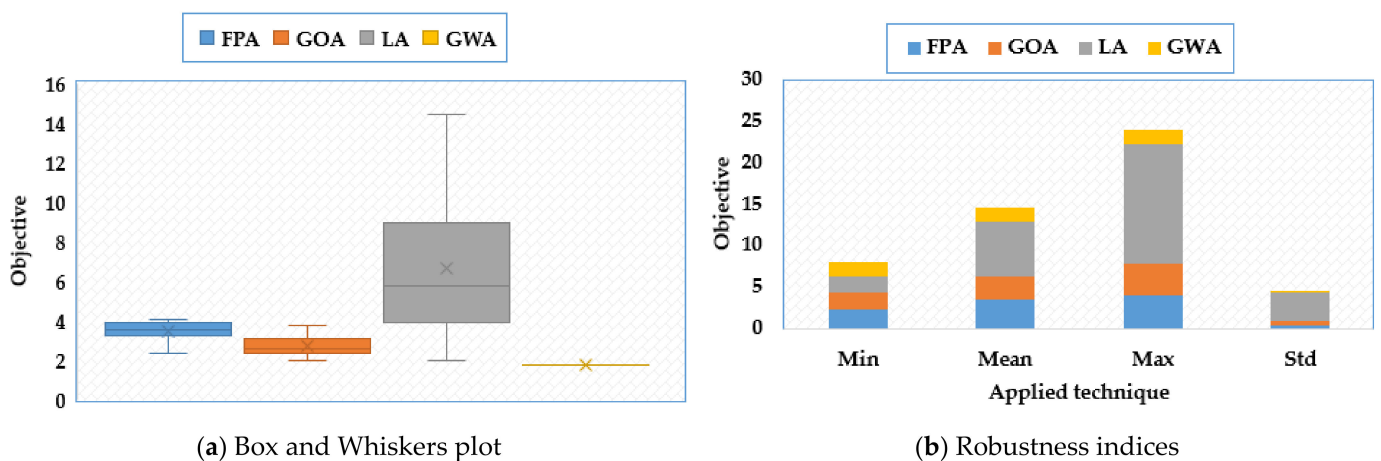


Figure 15. Statistical assessment of GWA, FPA, LA, and GOA for WBD under first case.

4.2.2. Second Case: Minimizing the Deflection

GWA, FPA, LA, and GOA are implemented in this case to reduce manufacturing costs, and their optimum control variables and outcome fitness values are provided in Table 10. All of the strategies used successfully determine the optimal solution with a deflection value of 4.991×10^{-7} . The obtained values for bar height and bar thickness for all techniques are

10 inches and 5 inches, respectively. The differences in welding thickness and clamping bar length have no influence on the deflection target as they are functions of the other two variables as specified in Equation (25). Figure 16 shows a statistical assessment of GWA, FPA, LA, and GOA for WBD problem under the first case. All compared techniques provide similar effective performance where the minimum, mean, and maximum are equivalent with $4.991E-07$.

Table 10. Optimal results of the GWA, FPA, LA, and GOA for TLSM design under first case.

Control Variables	FPA	GOA	LA	GWA
x_1 (inch)	4.2881	1.6449	0.5406	4.2948
x_2 (inch)	2.3619	9.2877	6.1552	3.4059
x_3 (inch)	10	10	10	10
x_4 (inch)	5	5	5	5
F_2 (Deflection)	4.99097×10^{-7}	4.99097×10^{-7}	4.99097×10^{-7}	4.99097×10^{-7}

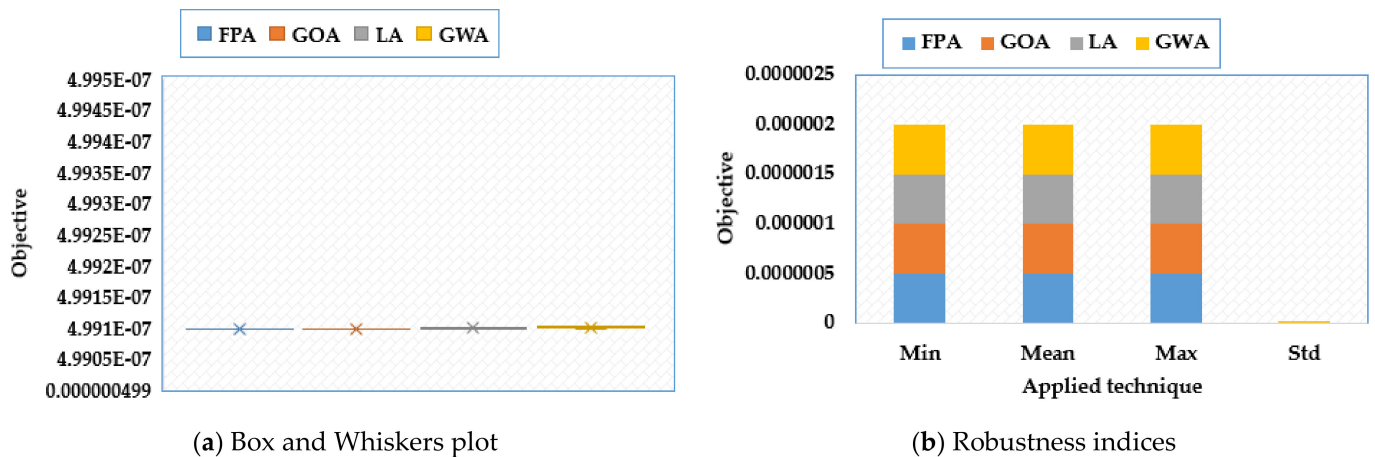


Figure 16. Statistical assessment of GWA, FPA, LA, and GOA for WBD under second case.

4.2.3. Third Case: Simultaneous Minimization of the Manufacturing Cost and Deflection

The multi-objective WBD optimization problem is studied in the third case. Figure 17 depicts the relevant Pareto fronts for the developed MGWO, MFPA, MOLA, and MGOA using four distinct reference points. Table 11 illustrates the hypervolume indicators of the produced MGWO, MFPA, MOLA, and MGOA for the WBD problem under the third scenario using the four reference points shown in Figure 17. As demonstrated, the developed MGWO provides the best performance. In comparison to the MFPA, the developed MGWO improves by 2.92%, 3.969%, 1.81%, and 2.51% with reference points (40,0.01), (60,0.015), and (60,0.015), respectively. In comparison to the MGOA, the developed MGWO improves by 4.55%, 2.88%, 2.87%, and 1.85%, respectively, with the reference points. When compared to the MOLA, the developed MGWO improves by 0.983%, 0.714%, 0.615%, and 0.48%, respectively.

Table 11. Hypervolume indicators of MGWO, MFPA, MOLA, and MGOA for WBD problem under third case.

Reference Points	MFPA	MOLA	MGOA	Developed MGWO
(40,0.01)	0.7918375	0.8076335	0.77853	0.81565
Improvement	2.92%	0.983%	4.55%	-

Table 11. Cont.

Reference Points	MFPA	MOLA	MGOA	Developed MGWO
(40,0.015)	0.825984	0.853993	0.835322	0.860131
Improvement	3.969%	0.714%	2.88%	-
(60,0.01)	0.84685	0.85718	0.83772	0.86248
Improvement	1.81%	0.615%	2.87%	-
(60,0.015)	0.874533	0.892716	0.880395	0.897016
Improvement	2.51%	0.48%	1.85%	-

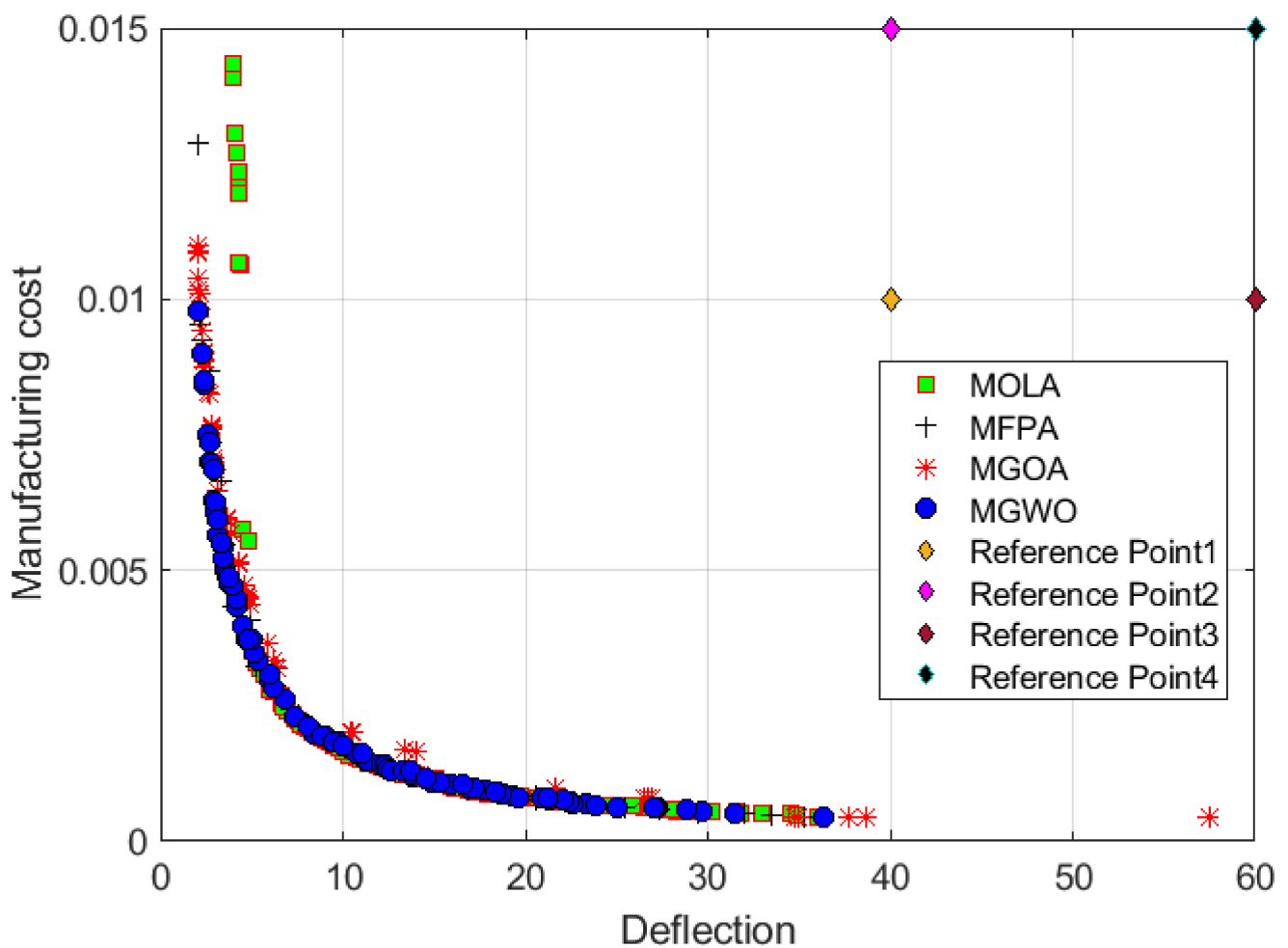
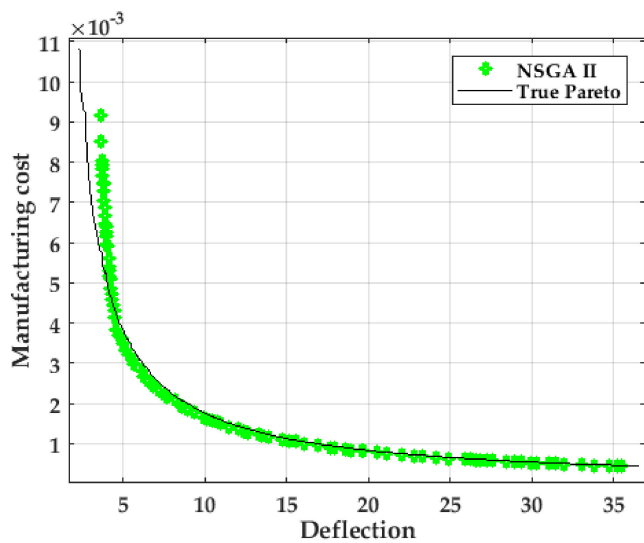


Figure 17. Obtained Pareto fronts of the developed MGWO, MFPA, MOLA, and MGOA for WBD under third case.

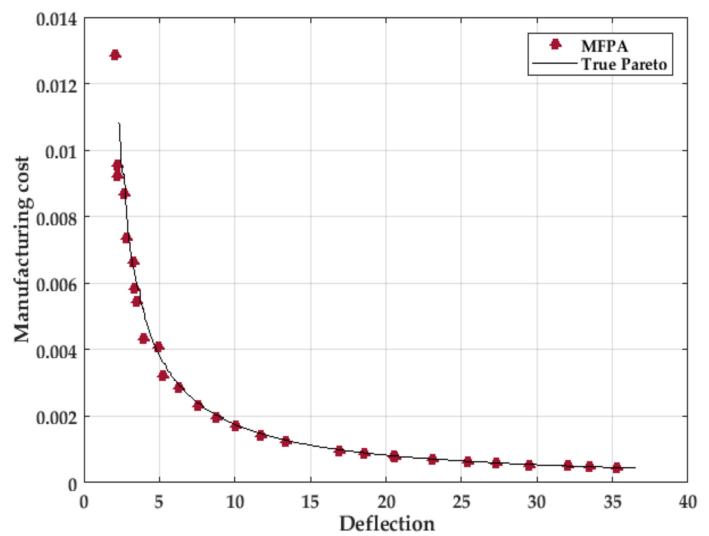
4.2.4. Comparative Assessment Considering Different Metrics

In this sub-section, a detailed comparative assessment considering different metrics presented in the literature, such as hypervolume, generational distance, inverted generational distance, spread, generalized-spread, and additive epsilon, considering the well-known bi-objective optimization problem of WBD, taking into account the true-Pareto front [57]. Figure 18 displays the obtained Pareto fronts versus true fronts of the developed MGWO, NSGA II, MFPA, MOLA, and MGOA for WBD under third case whilst Table 12 records the previous stated metrics. As shown, the proposed MGWO demonstrates greater efficiency where:

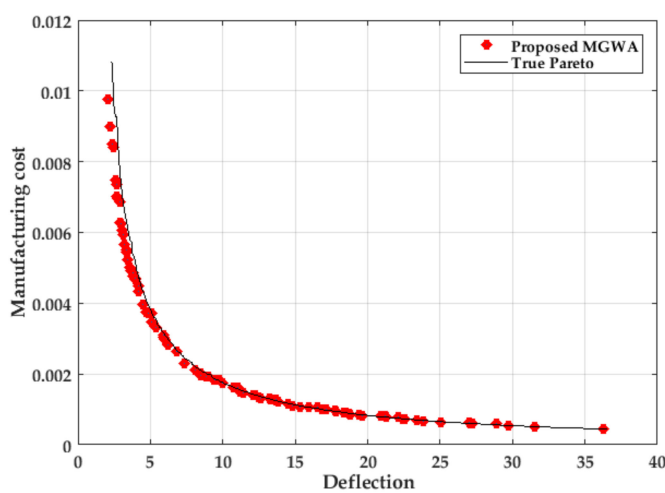
- The proposed MGWO provides the greatest hypervolume indicator of 0.326 while MFPA comes second with hypervolume indicator of 0.3227;
- The proposed MGWO achieves the least generational distance indicator of 0.0008, while NSGA II comes second with generational distance indicator of 0.0034;
- The proposed MGWO achieves the least inverted generational distance indicator of 0.00095, while MFPA comes second with generational distance indicator of 0.00121;
- In terms of the spread metric, the proposed MGWO achieves the least indicator value of 0.779, while MOLA and NSGA II come consecutively with 0.933 and 0.939, respectively;
- In terms of the additive epsilon metric, the proposed MGWO achieves the least indicator value of 0.000132.



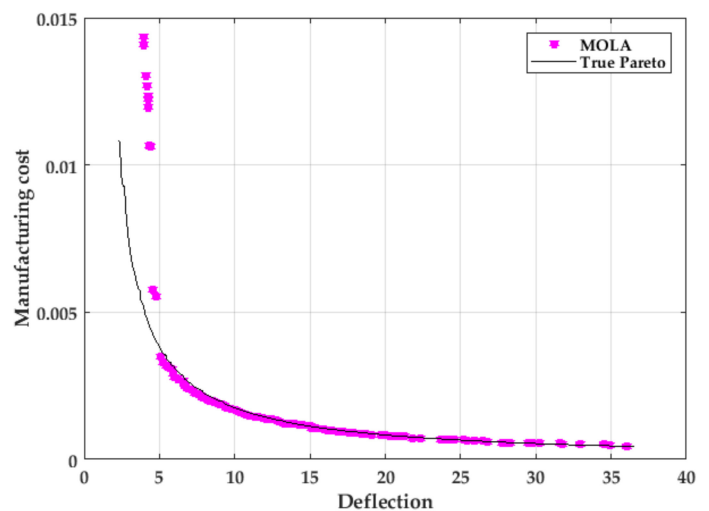
(a) NSGA II



(b) MFPA

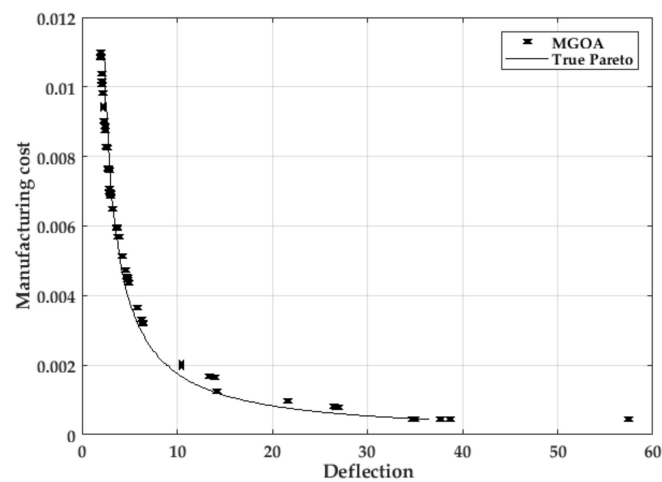


(c) Proposed MGWO



(d) MOLA

Figure 18. Cont.



(e) MGOA

Figure 18. Obtained Pareto fronts versus True—fronts of the developed MGWO, NSGA II, MFPA, MOLA, and MGOA for WBD under third case.

A closer accord to the comparison between the developed MGWO and NSGA II is shown in Figure 19. As shown in the sub-plot, the developed MGWO shows higher superiority, not only in finding better solutions in dominating solutions obtained by the well-known NSGA II, but also the true pareto front.

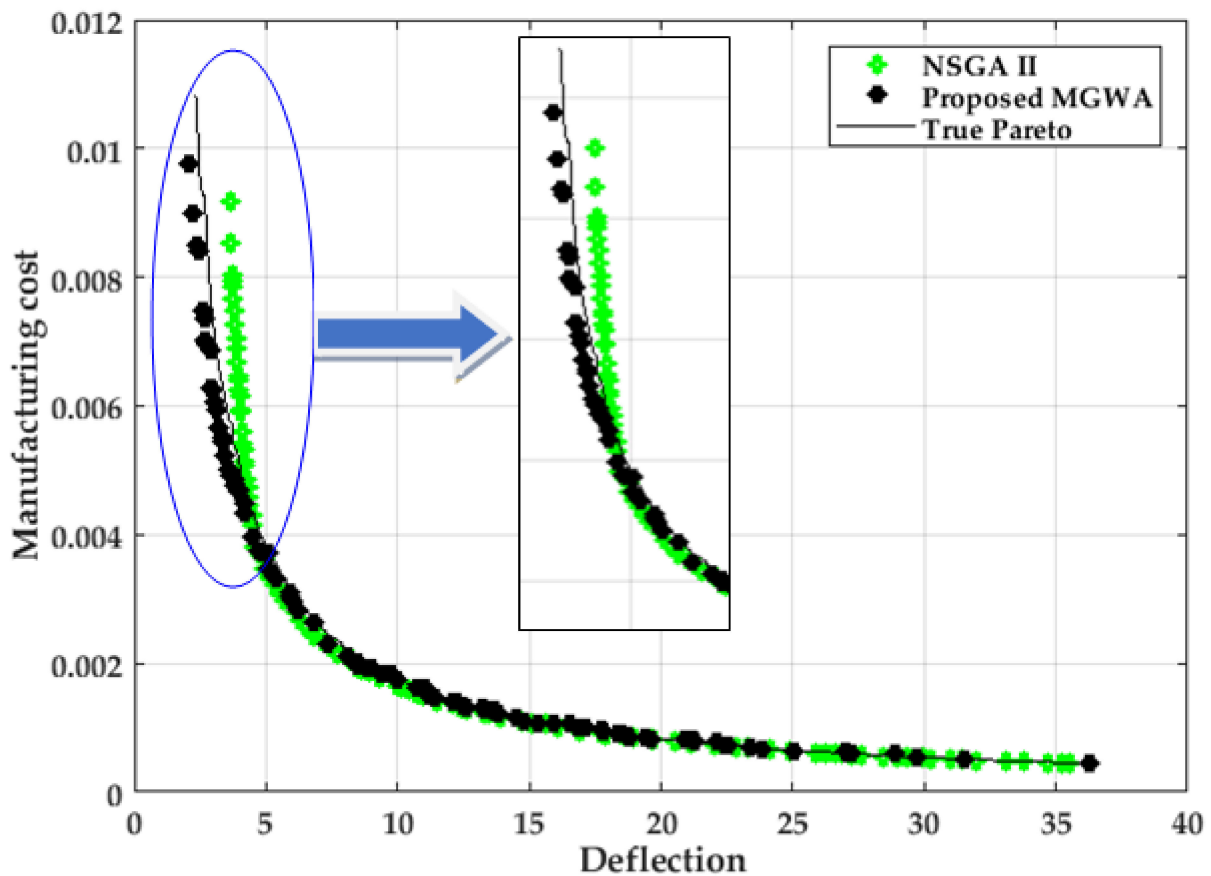


Figure 19. Obtained Pareto fronts versus True fronts of the developed MGWO and NSGA II for WBD.

Table 12. Comparative assessment considering different metrics of the compared algorithms for WBD problem.

	MGWO	NSGA II	MOLA	MFPA	MOGOA
Hypervolume	0.32627154	0.315202517	0.31532889	0.322732332	0.311235752
Generational distance	0.000823219	0.0034291	0.0060862	0.0028048	0.012417
Inverted generational distance	0.000950639	0.0013475	0.0014895	0.0012113	0.0028061
Spread	0.778953351	0.93986	0.93342	1.4189	1.2838
Generalized spread	0.830487363	0.87311	0.49653	1.4495	1.2676
Additive epsilon	0.000132346	1.8928	1.6185	0.00077754	0.0014939

5. Conclusions

This article suggests a developed the MGWO for the multi-objective shape design of tubular linear synchronous motors (TLSM). The multi-objective design of TLSM is handled by maximizing the operating force and minimizing the flux saturation. The developed MGWO is compared to several recent algorithms of MFPA, MOLA, and MGOA. Additionally, the validation of the developed MGWO is extended for a multi-objective form of welded beam design (WBD) by simultaneously minimizing the deflection and manufacturing costs. Moreover, considering single-objective optimization models for TLSM and WBD engineering problems, GWA, FPA, LA, and GOA are applied with a comparative assessment. The simulation results declare the superiority and effectiveness of the developed GWA over the others in achieving the single-objective minimization target. The satisfaction of all design constraints is guaranteed within their permissible limitations. A higher speed of convergence related to the employed GWA is also accompanied compared to the others. Moreover, considering the multi-objective optimization frameworks, the developed MGWO provides higher capability in acquiring non-dominated solutions with higher hypervolume indicators based on different reference points. Therefore, the developed MGWO demonstrates significant outperformance over MFPA, MOLA, and MGOA. As a result, the developed MGWO has shown promise in problem-solving capabilities when designing the TLSM and WBD. Furthermore, the proposed MGWO demonstrates greater efficiency and superiority versus true fronts of NSGA II, MFPA, MOLA, and MGOA for WBD based on different metrics presented in the literature, such as hypervolume, generational distance, inverted generational distance, spread, generalized-spread, and additive epsilon.

Author Contributions: Conceptualization, A.M., A.G. and A.S.; methodology, R.E.-S. and A.G.; software, A.M.; validation, R.E.-S. and S.F.A.-G.; formal analysis, R.E.-S. and S.F.A.-G.; investigation, A.M., A.G. and A.S resources, R.E.-S.; writing—original draft preparation, A.M., A.G. and A.S.; writing—review and editing, R.E.-S. and S.F.A.-G.; project administration, R.E.-S., funding acquisition, S.F.A.-G. All authors have read and agreed to the published version of the manuscript.

Funding: This work was supported by the Deanship of Scientific Research at King Khalid University through General Research Project under grant number (RGP.1/223/43).

Data Availability Statement: Not applicable.

Acknowledgments: The authors thank the Deanship of Scientific Research at King Khalid University for funding this work under Grant No. RGP.1/223/43.

Conflicts of Interest: The authors declare no conflict of interest.

Nomenclature

FPA	Flower Pollination Algorithm
GA	Genetic Algorithm
GOA	Grasshopper Optimization Algorithm
GWA	Grey Wolf Algorithm

LA	Lichtenberg Algorithm
MGWO	Multi-objective Grey Wolf Optimizer
MFPA	Multi-objective Flower Pollination Algorithm
MOLA	Multi-objective Lichtenberg Algorithm
MGOA	Multi-objective Grasshopper Optimization Algorithm
NSGA II	Non-dominated Sorting Genetic Algorithm II
PSO	Particle swarm optimization
TLSM	Tubular linear synchronous motors
WBD	Welded beam design

List of Symbols

k_F	Fill factor
B	Flux density
l	Length of magnetic pole
I	Conductor current
p	Number of poles
τ_p	Pole pitch
ins	Slot current
h_s	Height of the slot
h_m	Height of the magnet
t_s	Slot thickness
α, β, Δ and ω	Alpha, beta, delta, and omega wolves
N_w	Total number of the wolves in the pack
$Y_\Delta, Y_\beta, Y_\alpha$	Locations of the delta, beta, alpha are represented, respectively
$D_\Delta, D_\beta, D_\alpha$	Their accompanied distances
Y_{new}	Wolf's new location
Y	Current location of the wolf
r	Randomized value
a	Linear drop of the coefficient
It	Existing repetition
Mx_{It}	Ultimate repetition number
$Prob_j$	Probability choice for every hypercube
N	Total quantity of successful Pareto-optimal solutions
Fc	A fixed value bigger than one
PF	Penalty function
λ	A penalty factor
R_j	A binary coefficient

References

- Kennedy, J.; Eberhart, R. Particle swarm optimization. In Proceedings of the ICNN'95-International Conference on Neural Networks, Perth, WA, Australia, 27 November–1 December 1995; Volume 4, pp. 1942–1948. [\[CrossRef\]](#)
- Chou, J.S.; Truong, D.N. A novel metaheuristic optimizer inspired by behavior of jellyfish in ocean. *Appl. Math. Comput.* **2021**, *389*, 125535. [\[CrossRef\]](#)
- Shaheen, A.; El-Sehiemy, R.; Kamel, S.; Selim, A. Optimal Operational Reliability and Reconfiguration of Electrical Distribution Network Based on Jellyfish Search Algorithm. *Energies* **2022**, *15*, 6994. [\[CrossRef\]](#)
- Abualigah, L.; Yousri, D.; Elaziz, M.A.; Ewees, A.A.; Al-Qaness, M.A.; Gandomi, A.H. Aquila Optimizer: A novel meta-heuristic optimization Algorithm. *Comput. Ind. Eng.* **2021**, *157*, 107250. [\[CrossRef\]](#)
- El-Ela, A.A.A.; El-Sehiemy, R.A.; Shaheen, A.M.; Shalaby, A.S. Aquila Optimization Algorithm for Wind Energy Potential Assessment Relying on Weibull Parameters Estimation. *Wind* **2022**, *2*, 617–635. [\[CrossRef\]](#)
- Elshahed, M.; El-Rifaie, A.M.; Tolba, M.A.; Ginidi, A.; Shaheen, A.; Mohamed, S.A. An Innovative Hunter-Prey-Based Optimization for Electrically Based Single-, Double-, and Triple-Diode Models of Solar Photovoltaic Systems. *Mathematics* **2022**, *10*, 4625. [\[CrossRef\]](#)
- Naruei, I.; Keynia, F.; Molahosseini, A.S. Hunter-prey optimization: Algorithm and applications. *Soft Comput.* **2022**, *26*, 1279–1314. [\[CrossRef\]](#)
- Ginidi, A.; Elattar, E.; Shaheen, A.; Elsayed, A.; El-Sehiemy, R.; Dorrah, H. Optimal Power Flow Incorporating Thyristor-Controlled Series Capacitors Using the Gorilla Troops Algorithm. *Int. Trans. Electr. Energy Syst.* **2022**, *2022*, 9448199. [\[CrossRef\]](#)
- Hashim, F.A.; Houssein, E.H.; Hussain, K.; Mabrouk, M.S.; Al-Atabany, W. Honey Badger Algorithm: New metaheuristic algorithm for solving optimization problems. *Math. Comput. Simul.* **2022**, *192*, 84–110. [\[CrossRef\]](#)

10. El-Sehiemy, R.; Shaheen, A.; Ginidi, A.; Elhosseini, M. A Honey Badger Optimization for Minimizing the Pollutant Environmental Emissions-Based Economic Dispatch Model Integrating Combined Heat and Power Units. *Energies* **2022**, *15*, 7603. [[CrossRef](#)]
11. Koziel, S.; Michalewicz, Z. Evolutionary algorithms, homomorphous mappings, and constrained parameter optimization. *Evol. Comput.* **1999**, *7*, 19–44. [[CrossRef](#)]
12. Shaheen, A.M.; El-Sehiemy, R.; Farrag, S.M. A novel adequate bi-level reactive power planning strategy. *Int. J. Electr. Power Energy Syst.* **2016**, *78*, 897–909. [[CrossRef](#)]
13. Yuen, S.Y.; Lou, Y.; Zhang, X. Selecting evolutionary algorithms for black box design optimization problems. *Soft Comput.* **2019**, *23*, 6511–6531. [[CrossRef](#)]
14. Hashim, F.A.; Hussain, K.; Houssein, E.H.; Mabrouk, M.S.; Al-Atabany, W. Archimedes optimization algorithm: A new metaheuristic algorithm for solving optimization problems. *Appl. Intell.* **2021**, *51*, 1531–1551. [[CrossRef](#)]
15. Khan, R.A.; Farooqui, S.A.; Sarwar, M.I.; Ahmad, S.; Tariq, M.; Sarwar, A.; Zaid, M.; Ahmad, S.; Mohamed, A.S.N. Archimedes optimization algorithm based selective harmonic elimination in a cascaded h-bridge multilevel inverter. *Sustainability* **2022**, *14*, 310. [[CrossRef](#)]
16. Bouchekara, H.R.E.H. Electromagnetic device optimization based on electromagnetism-like mechanism. *Appl. Comput. Electromagn. Soc. J.* **2013**, *28*, 241–248.
17. Erol, O.K.; Eksin, I. A new optimization method: Big Bang-Big Crunch. *Adv. Eng. Softw.* **2006**, *37*, 106–111. [[CrossRef](#)]
18. Rashedi, E.; Nezamabadi-Pour, H.; Saryazdi, S. GSA: A Gravitational Search Algorithm. *Inf. Sci.* **2009**, *179*, 2232–2248. [[CrossRef](#)]
19. Hashim, F.A.; Houssein, E.H.; Mabrouk, M.S.; Al-Atabany, W.; Mirjalili, S. Henry gas solubility optimization: A novel physics-based algorithm. *Futur. Gener. Comput. Syst.* **2019**, *101*, 646–667. [[CrossRef](#)]
20. Askari, Q.; Saeed, M.; Younas, I. Heap-based optimizer inspired by corporate rank hierarchy for global optimization. *Expert Syst. Appl.* **2020**, *161*, 113702. [[CrossRef](#)]
21. Zou, F.; Wang, L.; Hei, X.; Chen, D. Teaching-learning-based optimization with learning experience of other learners and its application. *Appl. Soft Comput. J.* **2015**, *37*, 725–736. [[CrossRef](#)]
22. Talatahari, S.; Kaveh, A.; Sheikholeslami, R. Chaotic imperialist competitive algorithm for optimum design of truss structures. *Struct. Multidiscip. Optim.* **2012**, *46*, 355–367. [[CrossRef](#)]
23. Bayzidi, H.; Talatahari, S.; Saraee, M.; Lamarche, C.-P. Social Network Search for Solving Engineering Optimization Problems. *Comput. Intell. Neurosci.* **2021**, *2021*, 8548639. [[CrossRef](#)] [[PubMed](#)]
24. Tanabe, R.; Ishibuchi, H. An easy-to-use real-world multi-objective optimization problem suite. *Appl. Soft Comput. J.* **2020**, *89*, 106078. [[CrossRef](#)]
25. Nedjah, N.; Mourelle, L.D.M. Evolutionary multi-objective optimisation: A survey. *Int. J. Bio-Inspired Comp.* **2015**, *7*, 1–25. [[CrossRef](#)]
26. El-Ela, A.A.A.; El-Sehiemy, R.A.; Shaheen, A.M.; Ellien, A.R. Multiobjective coyote optimization algorithm for techno-economic simultaneous placement of DGs and FCLs in distribution networks. *Int. Trans. Electr. Energy Syst.* **2021**, *31*, e13050. [[CrossRef](#)]
27. Shaheen, A.M.; El-Sehiemy, R.A.; Alharthi, M.M.; Ghoneim, S.S.; Ginidi, A.R. Multi-objective jellyfish search optimizer for efficient power system operation based on multi-dimensional OPF framework. *Energy* **2021**, *237*, 121478. [[CrossRef](#)]
28. Premkumar, M.; Jangir, P.; Sowmya, R.; Alhelou, H.H.; Heidari, A.A.; Chen, H. MOSMA: Multi-Objective Slime Mould Algorithm Based on Elitist Non-Dominated Sorting. *IEEE Access* **2021**, *9*, 3229–3248. [[CrossRef](#)]
29. Sarhan, S.; Shaheen, A.; El-Sehiemy, R.; Gafar, M. A Multi-Objective Teaching-Learning Studying-Based Algorithm for Large-Scale Dispatching of Combined Electrical Power and Heat Energies. *Mathematics* **2022**, *10*, 2278. [[CrossRef](#)]
30. Li, L.; He, D.; Jin, J.; Yu, B.; Gao, X. Multi-objective load dispatch control of biomass heat and power cogeneration based on economic model predictive control. *Energies* **2021**, *14*, 762. [[CrossRef](#)]
31. Rizk-Allah, R.M.; El-Sehiemy, R.A.; Deb, S.; Wang, G.-G. A novel fruit fly framework for multi-objective shape design of tubular linear synchronous motor. *J. Supercomput.* **2017**, *73*, 1235–1256. [[CrossRef](#)]
32. Rao, R.V.; Waghmare, G. A new optimization algorithm for solving complex constrained design optimization problems. *Eng. Optim.* **2017**, *49*, 60–83. [[CrossRef](#)]
33. Arora, S.; Singh, S.; Yetilmezsoy, K. A modified butterfly optimization algorithm for mechanical design optimization problems. *J. Braz. Soc. Mech. Sci. Eng.* **2018**, *40*, 21. [[CrossRef](#)]
34. Yang, X.-S.; Karamanoglu, M.; He, X. Flower pollination algorithm: A novel approach for multiobjective optimization. *Eng. Optim.* **2014**, *46*, 1222–1237. [[CrossRef](#)]
35. Pereira, J.L.J.; Oliver, G.A.; Francisco, M.B.; Cunha, S.S., Jr.; Gomes, G.F. Multi-objective lichtenberg algorithm: A hybrid physics-based meta-heuristic for solving engineering problems. *Expert Syst. Appl.* **2022**, *187*, 115939. [[CrossRef](#)]
36. Mirjalili, S.Z.; Mirjalili, S.; Saremi, S.; Faris, H.; Aljarah, I. Grasshopper optimization algorithm for multi-objective optimization problems. *Appl. Intell.* **2018**, *48*, 805–820. [[CrossRef](#)]
37. Wang, C.; Li, X.; Wang, Z. Bilevel Multi-Objective Gray Wolf Algorithm Based on Packet Transport Network Optimization. *IEEE Access* **2021**, *9*, 162792–162804. [[CrossRef](#)]
38. Hao, P.; Sobhani, B. Application of the improved chaotic grey wolf optimization algorithm as a novel and efficient method for parameter estimation of solid oxide fuel cells model. *Int. J. Hydrogen Energy* **2021**, *46*, 36454–36465. [[CrossRef](#)]
39. Zhou, J.; Huo, X.; Xu, X.; Li, Y. Forecasting the carbon price using extreme-point symmetric mode decomposition and extreme learning machine optimized by the grey Wolf optimizer algorithm. *Energies* **2019**, *12*, 950. [[CrossRef](#)]

40. Yu, X.-W.; Huang, L.-P.; Liu, Y.; Zhang, K.; Li, P.; Li, Y. WSN node location based on beetle antennae search to improve the gray wolf algorithm. *Wirel. Netw.* **2022**, *28*, 539–549. [[CrossRef](#)]
41. Qin, W.; Wang, L.; Liu, Y.; Xu, C. Energy consumption estimation of the electric bus based on grey wolf optimization algorithm and support vector machine regression. *Sustainability* **2021**, *13*, 4689. [[CrossRef](#)]
42. El-Ela, A.A.A.; El-Sehiemy, R.A.; Shaheen, A.M.; Eissa, I.A. Optimal coordination of static VAR compensators, fixed capacitors, and distributed energy resources in Egyptian distribution networks. *Int. Trans. Electr. Energy Syst.* **2020**, *30*, e12609. [[CrossRef](#)]
43. Yang, L.; Ding, B.; Liao, W.; Li, Y. Identification of Preisach Model Parameters Based on an Improved Particle Swarm Optimization Method for Piezoelectric Actuators in Micro-Manufacturing Stages. *Micromachines* **2022**, *13*, 698. [[CrossRef](#)] [[PubMed](#)]
44. Ding, B.; Yang, Z.-X.; Zhang, G.; Xiao, X. Optimum design and analysis of flexure-based mechanism for non-circular diamond turning operation. *Adv. Mech. Eng.* **2017**, *9*, 168781401774335. [[CrossRef](#)]
45. Coello, C.A.C.; Toscano-Pulido, G.T.; Lechuga, M.S. Handling multiple objectives with particle swarm optimization. *IEEE Trans. Evol. Comput.* **2004**, *8*, 256–279. [[CrossRef](#)]
46. Rigelsford, J. Linear Synchronous Motors: Transportation and Automation Systems. *Assem. Autom.* **2000**, *20*. [[CrossRef](#)]
47. Mousa, A.A.; El-Wahed, W.F.A.; Rizk-Allah, R.M. A hybrid ant colony optimization approach based local search scheme for multiobjective design optimizations. *Electr. Power Syst. Res.* **2011**, *81*, 1014–1023. [[CrossRef](#)]
48. Pradhan, M.; Roy, P.K.; Pal, T. Grey wolf optimization applied to economic load dispatch problems. *Int. J. Electr. Power Energy Syst.* **2016**, *83*, 325–334. [[CrossRef](#)]
49. Singh, D.; Dhillon, J.S. Ameliorated grey wolf optimization for economic load dispatch problem. *Energy* **2019**, *169*, 398–419. [[CrossRef](#)]
50. Geleta, D.K.; Manshahia, M.S.; Vasant, P.; Banik, A. Grey wolf optimizer for optimal sizing of hybrid wind and solar renewable energy system. *Comput. Intell.* **2020**, *38*, 1133–1162. [[CrossRef](#)]
51. Mirjalili, S.; Saremi, S.; Mirjalili, S.M.; Coelho, L.D.S. Multi-objective grey wolf optimizer: A novel algorithm for multi-criterion optimization. *Expert Syst. Appl.* **2015**, *47*, 106–119. [[CrossRef](#)]
52. El-Sehiemy, R.; Hamida, M.A.; Elattar, E.; Shaheen, A.; Ginidi, A. Nonlinear Dynamic Model for Parameter Estimation of Li-Ion Batteries Using Supply-Demand Algorithm. *Energies* **2022**, *15*, 4556. [[CrossRef](#)]
53. Wang, X.; Yalaoui, F.; Dugardin, F. Non-dominated sorting genetic algorithms for a multi-objective resource constraint project scheduling problem. *J. Intell. Syst.* **2021**, *28*, 791–806. [[CrossRef](#)]
54. Majumder, S.; Barma, P.S.; Biswas, A.; Banerjee, P.; Mandal, B.K.; Kar, S.; Ziemba, P. On Multi-Objective Minimum Spanning Tree Problem under Uncertain Paradigm. *Symmetry* **2022**, *14*, 106. [[CrossRef](#)]
55. Qi, Z.; Kang, G.; Wu, X.; Sun, Y.; Wang, Y. Multi-objective optimization for selecting and siting the cost-effective BMPs by coupling revised GWLF model and NSGAI algorithm. *Water* **2020**, *12*, 235. [[CrossRef](#)]
56. Uray, E.; Carbas, S.; Geem, Z.W.; Kim, S. Parameters Optimization of Taguchi Method Integrated Hybrid Harmony Search Algorithm for Engineering Design Problems. *Mathematics* **2022**, *10*, 327. [[CrossRef](#)]
57. Mirjalili, S.; Jangir, P.; Mirjalili, S.Z.; Saremi, S.; Trivedi, I.N. Optimization of problems with multiple objectives using the multi-verse optimization algorithm. *Knowl. Based Syst.* **2017**, *134*, 50–71. [[CrossRef](#)]

Disclaimer/Publisher’s Note: The statements, opinions and data contained in all publications are solely those of the individual author(s) and contributor(s) and not of MDPI and/or the editor(s). MDPI and/or the editor(s) disclaim responsibility for any injury to people or property resulting from any ideas, methods, instructions or products referred to in the content.